Supporting Information

Photoactive Fe Catalyst for Light-Triggered Alkyd Paint Curing

Johan Bootsma,[a] Wesley R. Browne,[b] Jitte Flapper,[c] and Bas de Bruin[a]*

[a] Homogeneous, Supramolecular and Bio-Inspired Catalysis group, Van 't Hoff Institute for Molecular Sciences, University of Amsterdam, Science Park 904, 1098 XH Amsterdam, The Netherlands

[b] Molecular Inorganic Chemistry group, Stratingh Institute for Chemistry, University of Groningen, Nijenborgh 4, 9747 AG Groningen, The Netherlands

[c] Akzo Nobel Decorative Coatings B.V., Rijksstraatweg 31, 2171 AJ Sassenheim, The Netherlands

* E-mail: b.debruin@uva.nl

Table of Contents

General synthetic and NMR considerations

The chemicals ferrocene (98%, Fisher Scientific), benzoylferrocene (98%), $AlCl_3$ (99%, Acros Chemicals), aluminium powder (99.97%, Fisher Scientific), benzene (TCI), NH_4PF_6 (Fluorochem), $LiAlH_4$ (2.4M in THF, Fisher Scientific), methyl linoleate (99%, Fisher Scientific), phenyl-*N*-t-butylnitrone (PBN; Alfa Aesar, 98%) and 5,5-dimethyl-1-pyrrolidine-*N*-oxide (DMPO; ABCR, 97%) were obtained commercially and used without any further purification. Methyl linoleate was stored in a refrigerator (5 °C) until use; PBN and DMPO were stored in a freezer (-18 °C) inside a dinitrogen filled glovebox until use. THF (anhydrous) was tapped from an MBraun solvent purification system (MB SPS-800, with standard MBraun drying columns). The compounds [(Cp)Fe(C_6H_6)](PF_6) (**1**) and [(Cp)Fe(Ch)] (**2**) were obtained according to (modified) literature procedures,[1] as described below; the compounds [(Cp)Fe(C_6H_5Me)](PF_6) (**1'**) and [(Cp)Fe(Ch')] (**2'**) can be obtained similarly.[2] *d*-chloroform (Eurisotop), d_6-acetone (Eurisotop), d_3-acetonitrile (Sigma Aldrich) and d_6-benzene (Sigma Aldrich) were used as received. NMR spectra were recorded on a Bruker AMX 400 spectrometer at room temperature. NMR chemical shifts are reported in ppm and are referenced internally to the residual solvent peak ($CDCl_3$: δ = 7.26 ppm, $(CD_3)_2CO$: δ = 2.05 ppm, CD_3CN: δ = 1.94 ppm, C_6D_6: δ = 7.16 ppm for ^{1}H NMR). Individual peaks are reported as: multiplicity (s = singlet, d = doublet, t = triplet, dt = doublet of triplets), integration, coupling constant (J) in Hz.

Syntheses

[(Cp)Fe(C_6H_6)](PF_6) (1)

A 500 mL round bottom flask was charged with ferrocene (200.00 g, 107.5 mmol), aluminium powder (3.00 g, 111 mmol) and 120 mL benzene under air. 2.00 mL water (111 mmol) was added with vigorous stirring, followed by portion-wise addition of $AlCl_3$ powder (40.0 g, 301 mmol) over a few minutes. Note that a large egg-shaped stir bar is required to mix the heterogeneous reaction mixture effectively. The colour of the reaction mixture darkens (to green) and the mixture warms. A reflux condenser was attached and the mixture was heated at reflux for 60-80 min, while open to the air but shielded from light by wrapping it in aluminium foil. After cooling to room temperature, the brown reaction mixture was cooled to 0 °C in a water/ice mixture. Under strong stirring, pre-cooled water (0 °C) was added slowly. (Note: this can lead to a vigorous reaction and formation of big chunks of $Al(Cl)_x(OH)_y$ initially.) After a total of 150 mL water was added, the green aqueous layer was separated from the brown organic layer. Subsequently, under strong stirring a solution of NH_4PF_6 (22.15 g, 135.9 mmol) in 90 mL of water was added dropwise to the aqueous layer using a dropping funnel, leading to the formation of a green-yellow precipitate. The precipitate was isolated by filtration and washed with water (2x 25 mL); the resulting wet 'cake' on the filter was redissolved in 80 mL acetone. This solution was dried (Na_2SO_4) and drying agent removed by filtration. 240 mL of diethyl ether was added dropwise to the filtrate with vigorous stirring, leading to the formation of a yellow precipitate. The precipitate was isolated by filtration and washed with diethyl ether (2x 25 mL). The material was dried in air followed by drying under vacuum, giving 22.95 g of a fine yellow powder (MW: 344.02 g/mol; 66.7 mmol, 62%).

^{1}H NMR (400 MHz, $(CD_3)_2CO$): δ/ppm = 6.49 (s, 6H, η^6-C_6H_6), 5.24 (s, 5H, η^5-C_5H_5).

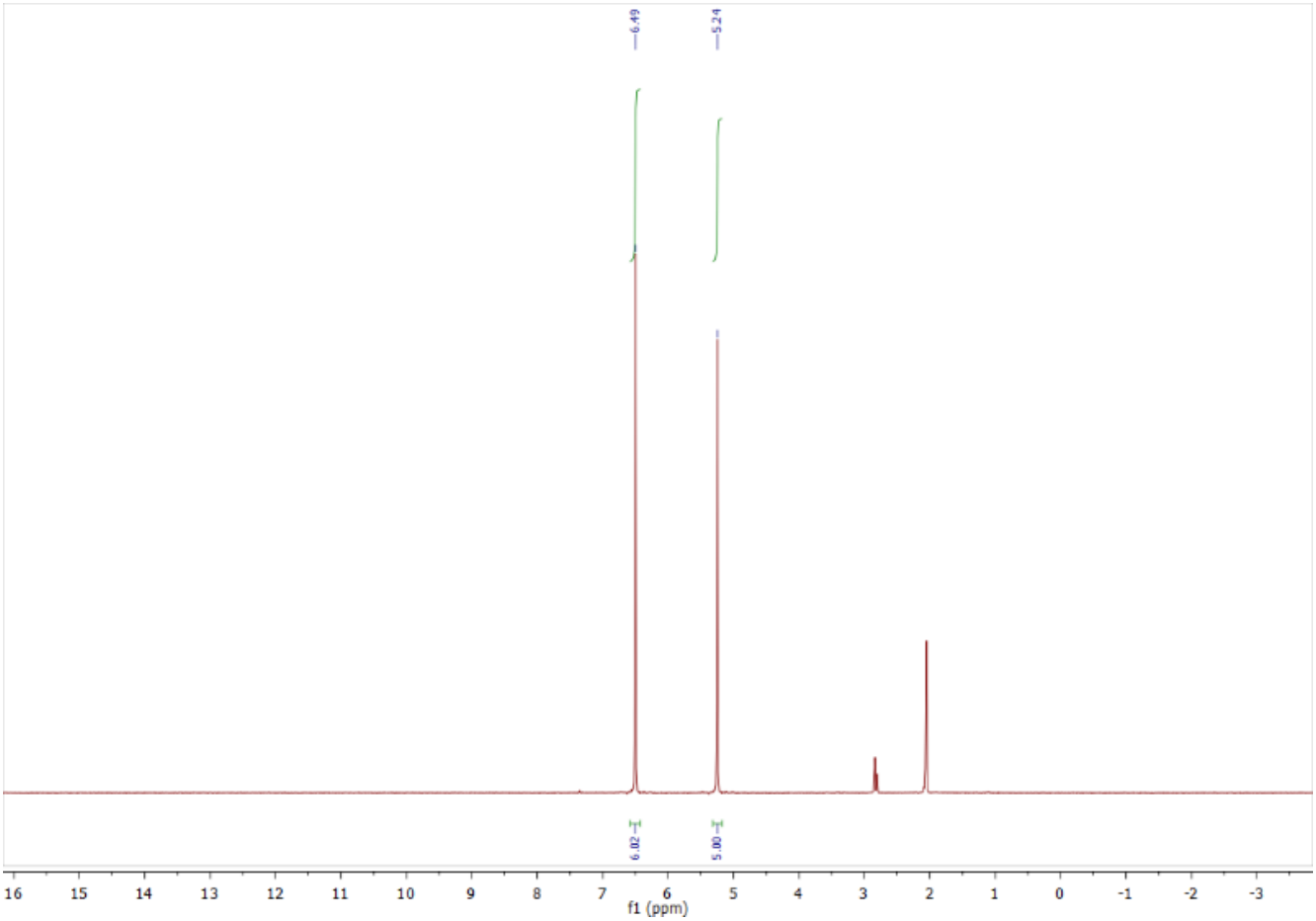

Figure S1. ^{1}H NMR spectrum (400 MHz, acetone-d_6) of [(Cp)Fe(C_6H_6)](PF_6) (**1**).

[(Cp)Fe(Ch)] (2)

[(Cp)Fe(C_6H_6)](PF_6) (4.00 g, 11.6 mmol) and 80 mL dry THF were added to a flame-dried 200 mL Schlenk flask under N_2 atmosphere. Under stirring, a 2.4 M solution of $LiAlH_4$ in THF (6.0 mL, 14.4 mmol; 1.2 eq.) was added dropwise over ~5 min. During this time the yellow suspension changed into a clear, dark red solution. (Note: after the addition the solution warms up slowly.) After 15 min the reaction mixture was cooled in an ice/water bath. Dropwise addition of 2.0 mL ethanol lead to bubble formation. A second 2.0 mL of ethanol was added followed by dropwise addition of 2.0 mL water. Another 2.0 mL water was added, followed by 100 mL heptane, and the contents of the reaction flask were transferred to a separatory funnel with 50 mL water. The red organic layer was separated, dried (Na_2SO_4), filtered and the volatiles from the filtrate removed in vacuo, leaving a red solid. This red solid was dissolved in pentane and the solution was filtered, and the volatiles subsequently removed in vacuo. The residue was dried under vacuum, yielding 1.86 g of a red solid (MW: 200.06 g/mol; 9.30 mmol, 80%).

Alternatively, [(Cp)Fe(C_6H_6)](PF_6) (2.20 g, 6.4 mmol), $NaBH_4$ (800 mg, 21.1 mmol) and 100 mL dry THF were added to a flame-dried 200 mL Schlenk flask under N_2 atmosphere. After the addition of three drops of water the reaction flask was placed in a 40 °C oil bath and covered with aluminium foil. After 17 h (overnight), the reaction flask was allowed to cool down to room temperature, then cooled on in ice/water bath. The excess of borohydride was quenched using 2.0 mL water (dropwise); after 5 minutes the flask was allowed to come to room temperature. The contents were poured in a 500 mL separatory flask, together with 100 mL water and 100 mL heptane. After shaking and separating the layers, the red organic layer was dried (Na_2SO_4), filtered and the volatiles from the filtrate removed in vacuo, leaving a red solid. This red solid was dissolved in pentane and the solution was filtered, and the volatiles subsequently removed in vacuo. The residue was dried under vacuum, yielding 1.27 g of a red solid (MW: 200.06 g/mol; 6.35 mmol, 99%).

^{1}H NMR (400 MHz, C_6H_6): δ/ppm = 5.89 (t, *J* = 4.7 Hz, 1H, C**H**CHCHCH_2), 4.09* (t, *J* = 4.8 Hz, 2H, CHC**H**CHCH_2), 4.07* (s, 5H, η^5-C_5H_5), 2.47 (dt, *J* = 12.6, 6.5 Hz, 1H, CHCHCHC**H**$_2$-*endo*), 2.04 (t, *J* = 6.1 Hz, 2H, CHCHC**H**CH_2), 1.71 (d, J = 12.4 Hz, 1H, CHCHCHC**H**$_2$-*exo*). *The peaks at 4.09 (t) and 4.07 (s) overlap.

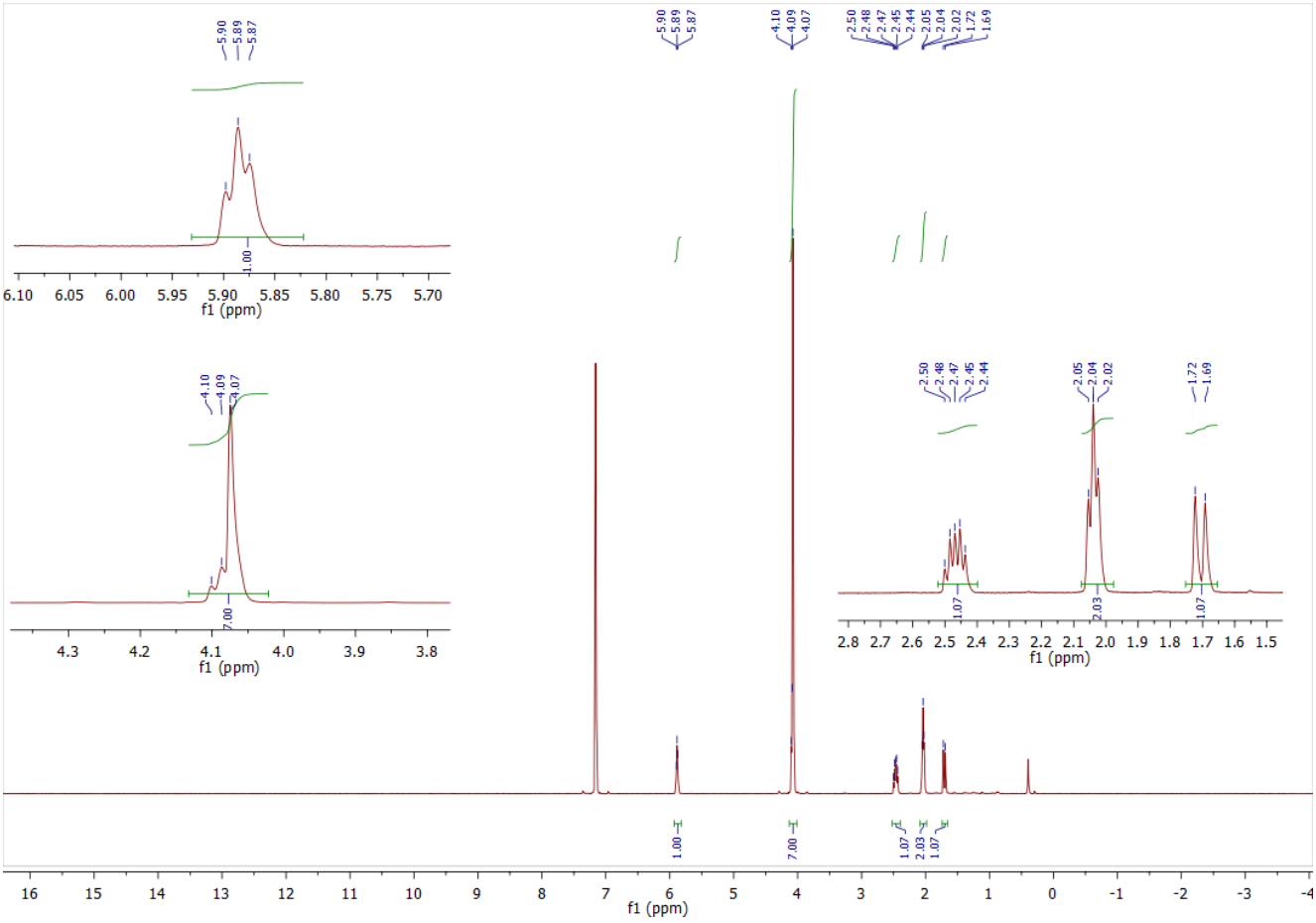

Figure S2. ^{1}H NMR spectrum (400 MHz, benzene-d_6) of [(Cp)Fe(Ch)] (**2**).

Coating Formulations

General considerations

The alkyd solution Setal-270 SM-70 was obtained from Allnex (formerly Nuplex Resins). It is an alkyd solution based on soybean oil containing 70 wt% solids, the remainder being hydrotreated naphtha; the 70 wt% alkyd resin itself is produced from soybean oil (65% by mass), phthalic anhydride (25% by mass) and pentaerythritol (10% by mass). Co(neodecanoate)$_2$ (CoNeo, **3**) was obtained from Venator, as a solution of cobalt neodecanoate in de-aromatised kerosine containing 10% cobalt by mass, sold under the name Durham Nuodex Cobalt 10 Neo. [(Me$_3$TACN)$_2$Mn$_2$(μ-OOCR)$_3$](OOCR) (Mn/MeTACN, **4**) (OOCR = acetate[3] or 2-ethylhexaoate[4]) was obtained from Venator, as a solution of the complex of the Mn^{II} carboxylate and Me$_3$TACN in 2-ethylhexanol and de-aromatised kerosine containing 1% manganese by mass, sold under the name Nuodex DryCoat. The calcium and zirconium carboxylates Valirex Ca5 (product name: Valirex Ca 5%, Umicore Specialty Materials) and Nuodex Zr18 (product name: Durham Nuodex Zirconium 18, Venator) are solutions of calcium 2-ethyl hexanoate and zirconium 2-ethyl hexanoate in de-aromatised white spirits D60 or de-aromatised kerosene containing 5% calcium and 18% zirconium by mass, respectively. The anti-skinning agent 2-butanone oxime (product name: Exkin 2) was obtained from Venator.

Paint mixing

Standard formulation consists of mixing these components in the following manner:

Setal 270	:	79.04 wt%
Valirex Ca5	:	2.76 wt%
Nuodex Zr18	:	2.76 wt%
Exkin2	:	0.50 wt%
Co 10 Neo or DryCoat	:	0.69 wt%
Exxsol D40 solvent	:	14.25 wt%
Total	:	100.00 wt%

If any ingredient was left out of the formulation, it was replaced with Exxsol D40 solvent. Alternatively, instead of Exxsol D40 an aliphatic solvent such as heptane was used for laboratory scale tests.

*Example: full formulation using Nuodex DryCoat (Mn/MeTACN, **4**)*

A metal can was charged with 79.04 g Setal-270. An overhead stirrer was lowered into the paint can and under stirring 2.76 g of Ca5 solution, 2.76 g of Zr18 solution, 0.50 g Exkin2, 0.69 g of Nuodex DryCoat solution and 14.25 g Exxsol D40 were added. After 1-2 minutes of additional stirring the overhead stirrer was removed and the can was closed using a metal lid. The paint mixture was left standing overnight at room temperature before it was applied for drying time and hardness measurements.

Manganese content: 0.69 g * 1 wt% Mn ≡ 6.9 mg Mn. As the 79.04 g Setal-270 is 70% solids by mass, this gives a total of 79.04*0.70 = 55.33 g of solids (solid binder content). Therefore, the wt% Mn on solids (solid binder content) is (6.9 mg / 55330 mg)*100 % = 0.0125 wt%.

*Example: small scale formulation (10 g) using Nuodex Cobalt 10 Neo (CoNeo, **3**), with 2-butanone oxime*

An amber vial containing 7.90 g Setal-270 and a small spatula was placed on the balance and tared. Afterwards 69 mg of Nuodex Cobalt 10 Neo solution was added, the mixture was stirred by spatula, followed by the addition of 50 mg Exkin2, after which it was stirred by spatula again. Heptane was added to a mass of 2.10 g (total mass = 7.90 + 2.10 = 10.00 g), after which it was stirred by spatula and stored in the dark. The paint mixture was left standing overnight at room temperature before it was applied for measurements.

Cobalt content: 69 mg * 10 wt% Co ≡ 6.9 mg Co. As the 7.90 g Setal-270 is 70% solids by mass, this gives a total of 7.90*0.70 = 5.53 g of solids (solid binder content). Therefore, the wt% Co on solids (solid binder content) is (6.9 mg / 5530 mg)*100% = 0.125 wt%.

*Example: small scale formulation (10 g) using [(Cp)Fe(Ch)] (**2**) (0.10 wt%), without 2-butanone oxime*

An amber vial containing 7.90 g Setal-270 and a small spatula was placed on the balance and tared. Afterwards 990 mg of a 2 wt% solution of [(Cp)Fe(Ch)] (**2**) in heptane was added, the mixture was stirred by spatula, and heptane was added to a mass of 2.10 g (total mass = 7.90 + 2.10 = 10.00 g), after which it was stirred by spatula and stored in the dark. The paint mixture was left standing overnight at room temperature before it was applied for measurements.

Iron content: 990 mg * 2 wt% solution ≡ 19.8 mg [(Cp)Fe(Ch)]. As the molecular weight of [(Cp)Fe(Ch)] is 200.06 g/mol, and the molecular weight of iron is 55.85 g/mol, the wt% Fe in [(Cp)Fe(Ch)] is (55.85 / 200.06)*100% = 27.9 wt%. Given this 27.9 %, the total amount of Fe is 19.8*0.279 = 5.52 mg Fe. Therefore, the wt% Fe on solids (solid binder content) is (5.52 mg / 5530 mg)*100% = 0.10 wt%.

Drying time measurements

Drying times were determined according to ASTM D5895-13 using a BK recorder (wet film thickness 90 µm). All paints were prepared on full formulation, i.e. with calcium and zirconium caboxylates and 2-butanone oxime. After the application of the film on a glass panel (300 x 25 mm), a vertical blunt needle, pressed upon by a 5 g load, was placed into the freshly applied film and then dragged in a straight line through the drying paint in the longitudinal direction of the panel. The so-called 'dry-hard time', i.e. when drying has proceeded sufficiently that the paint film is not displaced anymore (Stage III of drying in ASTM D5895-13) was determined for the paints within 1 day after preparation (initial) and after the paints had been stored at 35 °C for 2 weeks (aged). Drying times were determined at 10 °C and 85% relative humidity (light intensity: 190 Lux) and at 23 °C and 50% relative humidity (light intensity: 116 Lux). The drying at 10 °C was determined by applying the paint at 23 °C; immediately after application the painted glass strip was moved into a room with a temperature of 10 °C. The drying times that were obtained in this way are displayed in figure S3 (top left: curing at 10 °C, bottom left: curing at 23 °C). The data show that there is no loss of dry for paints dosed with [(Cp)Fe(Ch)] (**2**) after storage, and that drying times of 3-4 h which are obtained for paints cured with the commercial driers Nuodex Cobalt 10 Neo (CoNeo, **3**) and Nuodex DryCoat (Mn/MeTACN,, **4**) are also attainable for the [(Cp)Fe(Ch)] / $[(Cp)Fe(C_6H_6)]^+$ system.

For the initial set of measurements, in addition to samples exposed continuously to the light a set of samples was placed in the dark after application in the light. In all cases the samples dosed with [(Cp)Fe(Ch)] (0.010-0.20 wt%) (**2**) did not reach the end of Stage III of curing within 24h, regardless of temperature (10 or 23 °C). For the set of measurements on the aged paints, this procedure was repeated but now the samples were brought back into the light after 18 h (10 °C) or 24 h (23 °C) and left in the light for 24 h. In this case all paints dosed with [(Cp)Fe(Ch)] (**2**) (0.010-0.20 wt%) reached the end of Stage III within these 24 h in the light, showing the light-latency of the [(Cp)Fe(Ch)] / $[(Cp)Fe(C_6H_6)]^+$ system.

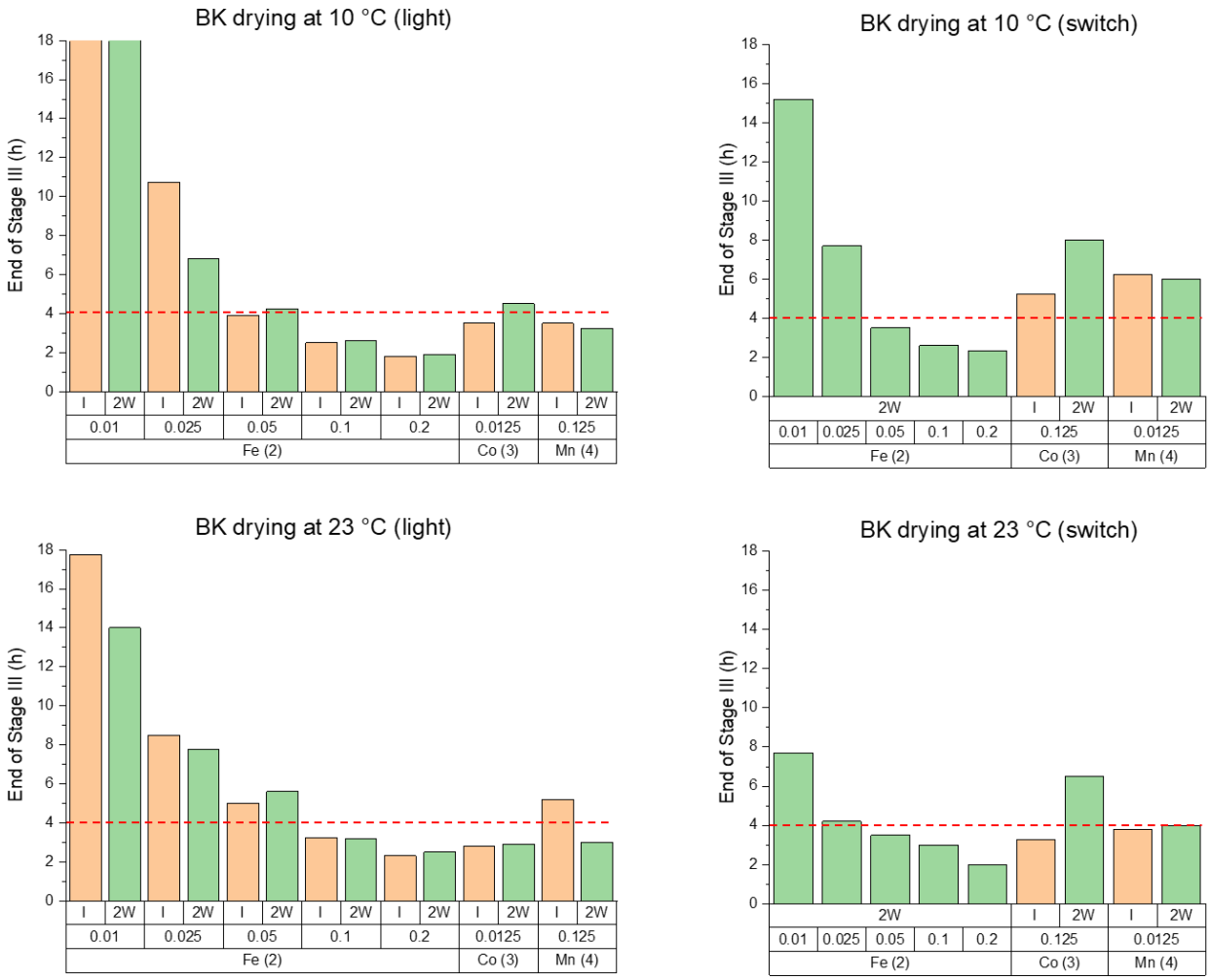

Figure S3. BK drying times (end of Stage III) for the initial set of measurements (I) and aged samples (2W), with the concentrations of drier expressed as wt% metal w.r.t solid binder material. A line has been drawn at 4 h to guide the eye. The paint dosed with [(Cp)Fe(Ch)] (**2**) at 0.010 wt% did not cure in the 24 h of the BK test at 10 °C (top left), but did cure within 18 h of the BK test at 23 °C (bottom left). After 18 h in the dark at 10 °C the glass slides coated with the aged paints were exposed to the light for 24 h (top right); the times shown here for [(Cp)Fe(Ch)] (**2**) are corrected for this (18 hours have been subtracted from the recorded drying times). After 24 h in the dark at 23 °C the glass slides coated with the aged paints were exposed to the light for 24 h (bottom right); the times shown here for [(Cp)Fe(Ch)] (**2**) are corrected for this (24 hours have been subtracted from the recorded drying times).

Hardness measurements

The König hardness of paint films was assessed using the pendulum damping test according to DIN53157. A glass panel was coated with a 90 µm wet film, held at 23 °C and 50% relative humidity and the hardness development in time was monitored with a König pendulum. The number of oscillations needed to reduce from an initial deflection of 6° to a deflection of 3° was measured. The average of duplicate measurements was recorded. The König hardness was measured after 1 day, 4 days, 7 days and 14 days of storage at 23 °C and 50% relative humidity. After 14 days, the films were exposed for a further 100 hours to a temperature of 50 °C in an oven and the König hardness was determined after an acclimatisation of 4 hours at 23 °C and 50% relative humidity.

Table S1. König hardness values (number of oscillations, average of duplicate) for coatings cured at 23 °C at 50 % relative humidity. For all concentrations of [(Cp)Fe(Ch)] (**2**) the König hardness value increases over time, even for the 0.010 wt% sample which had not fully cured after 1 day.

Drier	1 day	4 days	7 days	14 days	100h @ 50 °C
3 (CoNeo)	15	21.5	24.5	29.5	40
4 (Mn/MeTACN)	13	13	13	13	15
2 (0.010 wt%)	-	15	18	19	23
2 (0.025 wt%)	10	13.5	18.5	20	24.5
2 (0.050 wt%)	13	17	19	20.5	27
2 (0.10 wt%)	13	16	18.5	21.5	30.5
2 (0.20 wt%)	14	18.5	21.5	26.5	38.5

NMR studies

[(Cp)Fe(C_6H_6)](PF_6) (1) in degassed acetonitrile-d_3

Inside a dinitrogen filled glovebox [(Cp)Fe(C_6H_6)](PF_6) (**1**) (7.4 mg, $2.2 \cdot 10^{-2}$ mmol) was dissolved in 0.70 mL of acetonitrile-d_3 that had been degassed by three freeze-pump-thaw cycles, giving a light yellow transparent solution ($3.1 \cdot 10^{-2}$ M). The NMR tube was sealed with parafilm before removing it from the glovebox. The ^{1}H NMR spectrum showed signals at 6.23 ppm (6H, η^6-C_6H_6) and 5.02 ppm (5H, η^6-C_5H_5) corresponding to **1**. The NMR tube was held under laboratory lighting (indoor fluorescent beam lighting + outdoor sunlight through the lab window) and the ^{1}H NMR spectrum was recorded every hour, showing the appearance and increase of two new signals at 7.37 ppm (C_6H_6) and 4.15 ppm (ferrocene, Cp_2Fe) over time, at the cost of the signals corresponding to **1**. The conversion of photolysis was quantified as

$$\text{Residual } \mathbf{1}\ (\%) = \frac{\text{integral@6.23 ppm}}{\text{integral@6.23 ppm} + \text{integral@7.37 ppm}} \cdot 100\%$$

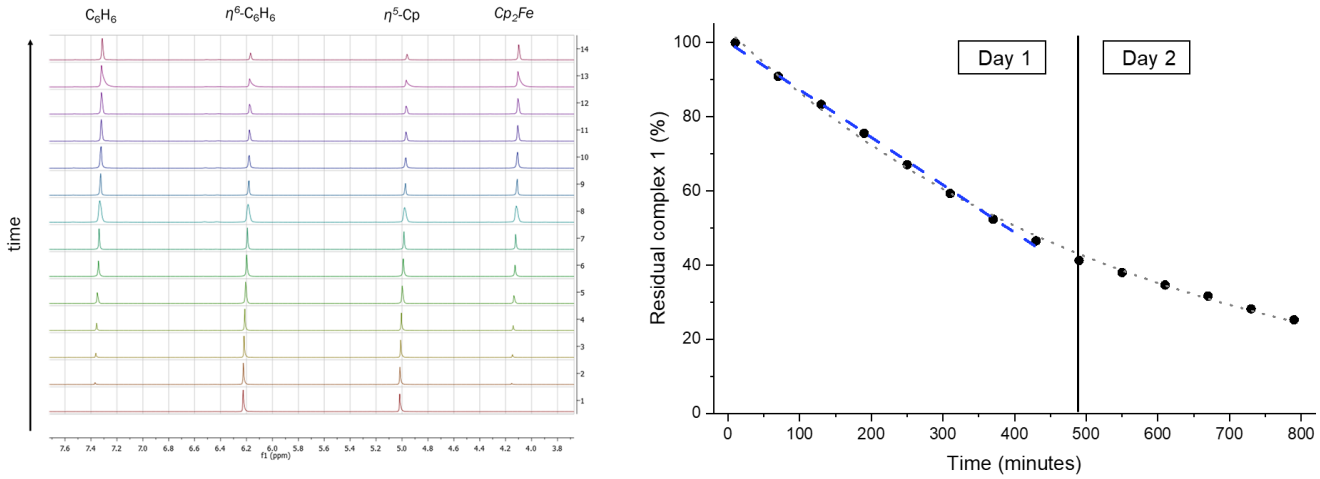

Figure S4. ^{1}H NMR spectroscopy following the photolysis of [(Cp)Fe(C_6H_6)](PF_6) (**1**) in acetonitrile-d_3 under laboratory light conditions. A spectrum was recorded at 1 hour intervals. Overall the data shows an exponential decrease (R^2 = 0.99); the data of the first seven hours show a linear decrease (R^2 = 0.99).

[(Cp)Fe(Ch)] (2) in degassed Setal-270 (1.5 wt% Fe)

A mixture of 15.80 g Setal-270 and 4.20 g heptane was degassed by three freeze-pump-thaw cycles before it was introduced to a dinitrogen filled glovebox. Inside the glovebox, a vial was charged with 2.00 g of the paint mixture and [(Cp)Fe(Ch)] (**2**) (59.4 mg, 1.5 wt% Fe w.r.t. solids). After mixing the contents of the vial by spatula, a ~60 mg sample was taken for ^{1}H NMR analysis ($CDCl_3$). Three other samples were prepared similarly with 2.00 g paint mixture each and either ferrocene (27.6 mg), benzene (23.2 mg) or sodium cyclopentadienide (NaCp, 26.2 mg). Each sample was stirred by spatula before ~60 mg of the mixture was taken for ^{1}H NMR analysis ($CDCl_3$). Additionally, ~60 mg of the paint mixture (without additive) was taken for ^{1}H NMR analysis ($CDCl_3$). (Note: these samples were prepared in the glovebox; the $CDCl_3$ used for the NMR analyses had been degassed by three freeze-pump-thaw cycles before it had been introduced into the glovebox.)

Inside of the glovebox, a syringe was loaded with part of the paint mixture that had been dosed with [(Cp)Fe(Ch) (**2**) at 1.5 wt%. Outside of the glovebox, an NMR tube was charged with ~60 mg of this paint mixture, using the syringe. The drop of paint was distributed over the inside NMR tube by swirling it, creating a thin film. The sample was left in the dark overnight, positioned horizontally, after which it was analysed by ^{1}H NMR ($CDCl_3$).

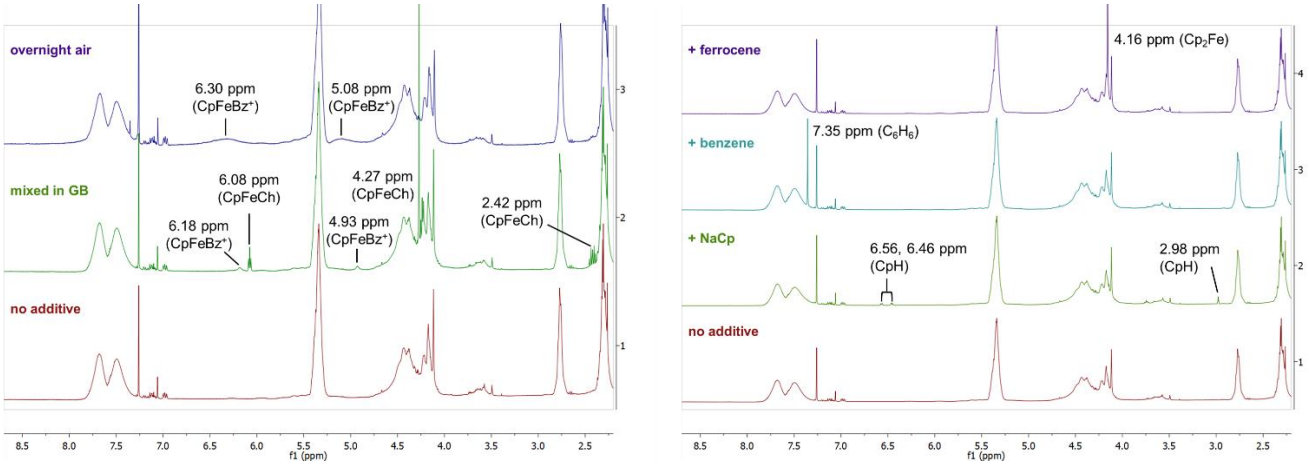

Figure S5. Left, from bottom to top: ^{1}H NMR spectra (400 MHz, $CDCl_3$) of Setal-270, Setal-270 with [(Cp)Fe(Ch)] (**2**) (1.5 wt%) mixed in a dinitrogen filled glovebox and a sample of Setal-270 with [(Cp)Fe(Ch)] (**2**) (1.5 wt%) that had been exposed to air overnight. Overnight storage leads to full oxidation of **2** to **1**, as indicated by the disappearance of the sharp signals at 6.08, 4.27 and 2.42 ppm, and the appearance of broadened signals at 6.30 and 5.08 ppm. Right, from bottom to top: ^{1}H NMR spectra (400 MHz, $CDCl_3$) of Setal-270, Setal-270 with NaCp added, Setal-270 with benzene added and Setal-270 with ferrocene added. The signals for benzene (7.35 ppm) and ferrocene (4.16 ppm) show up as clear singlets; mixing Setal-270 with NaCp leads to the formation of cyclopentadiene (CpH), as indicated by the resonances at 6.56, 6.46 and 2.98 ppm.

Inside the glovebox, a syringe was loaded with part of the paint mixture that had been dosed with [(Cp)Fe(Ch) (**2**) at 1.5 wt%. Outside of the glovebox, seven NMR tubes were each charged with ~60 mg of this paint mixture, using the syringe. The drops of paint were distributed over the inside of the NMR tubes by swirling it, creating a thin film. The samples were left in the dark overnight, positioned horizontally. The next day an NMR tube was placed on the laboratory bench every hour for six hours, positioned horizontally and rotated occasionally. One sample was left in the dark during all this time. At the end of the six hours all seven tubes were wrapped in aluminium foil and subsequently to all of them was added 0.60 mL $CDCl_3$. The tubes were shaken to dissolve the paint material, after which the samples were analysed by ^{1}H NMR spectroscopy.

To quantify the photo-activation, the *cis*-C**H**=C**H** resonance (5.34 ppm) of the fatty acid tails was used for normalisation, by setting the total concentration of C_6H_6-containing species before the photolysis ([(Cp)Fe(Ch)] + [[(Cp)Fe(C_6H_6)]$^+$, i.e. integral@6.08 ppm + integral@6.18 ppm) of the sample prepared in the glovebox to 100 and comparing with this the release of C_6H_6 (integral@7.35 ppm) after the air-oxidation and exposure to light. Spectral analysis was carried out using the program Spectragryph;[5] the integral values of the resonances at 7.35 ppm (C_6H_6), 6.18 ppm ([(Cp)Fe(C_6H_6)]$^+$, η^6-C_6H_6), 6.08 ppm ([(Cp)Fe(Ch)], η^6-C_6H_6) and 5.34 ppm (*cis*-CH=CH) were obtained from the raw data using the option Integration with Baseline within Spectragryph.

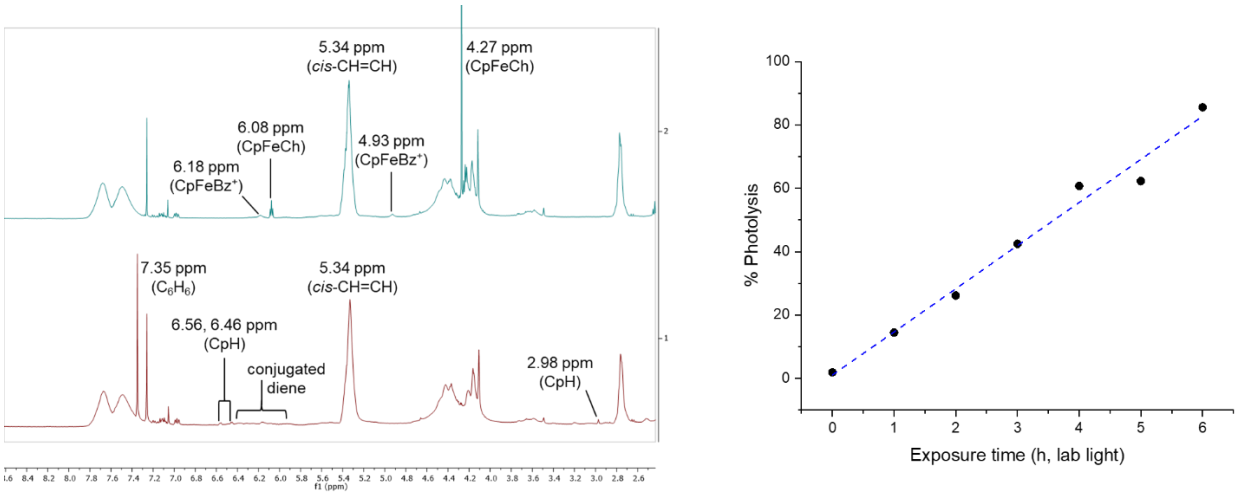

Figure S6. ^{1}H NMR spectra during the photolysis of $[(Cp)Fe(C_6H_6)]^+$ in Setal-270 under laboratory lighting conditions. Left: samples exposed to light show a release of C_6H_6 (7.35 ppm), but not formation of ferrocene (4.16 ppm – compare to Figure S5), shown here for the sample exposed to light for 4 h. Additionally, since only a small amount of free cyclopentadiene (CpH) has formed, this suggests the Cp ligand is still bound to the majority of the photo-activated $[(Cp)Fe(C_6H_6)]^+$. Right: the release of arene fits well to a linear trendline (R^2 = 0.98).

Both NMR studies show a linear decrease/increase over the period of photolysis, similar to the linear changes obtained in by FTIR spectroscopy (see below).

Model compound study using methyl linoleate

Four stock solutions were prepared:
- 10 wt% methyl linoleate in acetone-d_6
- 2.5 wt% $[(Cp)Fe(C_6H_6)](PF_6)$ (**1**) in acetone-d_6
- 2.5 wt% Nuodex Cobalt 10 Neo solution (CoNeo, **3**) in acetone-d_6
- 2.5 wt% Nuodex DryCoat solution (Mn/MeTACN, **4**) solution in acetone-d_6

Note: unlike at the drying time and hardness tests, the wt% concentrations given here do not express the wt% of metal used. For **1** the complex was dosed as a solid, so the 2.5 wt% is determined as mass solid / mass acetone-d_6. For **3** and **4** the stock solutions were made from the commercially available drier solutions, so the 2.5 wt% is determined as mass drier solution / mass acetone-d_6.

Four 20 mL clear vials were charged with 80 µL of the 10 wt% solution of methyl linoleate in acetone-d_6 each. To the vials was added 20 µL of one of the 2.5 wt% catalyst solutions in acetone-d_6, or 20 µL of acetone-d_6 for the control sample. The solutions were mixed by rotating the vials. The vials were left open (no cap; to allow evaporation of acetone-d_6) under ambient light. After six hours 0.60 mL of $CDCl_3$ was added to each vial and the resulting solutions were analysed by ^{1}H NMR spectroscopy.

Samples dosed with **3** and **4** show a higher conversion (Figure S7), as expressed by the decrease of the resonances at 5.34 ppm (*cis*-alkene, -CH_2-C**H**=C**H**-CH_2-C**H**=C**H**-CH_2-), 2.76 ppm (*bis*-allylic methylene, -CH_2-CH=CH-C**H**$_2$-CH=CH-CH_2-) and 2.04 ppm (*mono*-allylic methylene, -C**H**$_2$-CH=CH-CH_2-CH=CH-C**H**$_2$-).[6a]

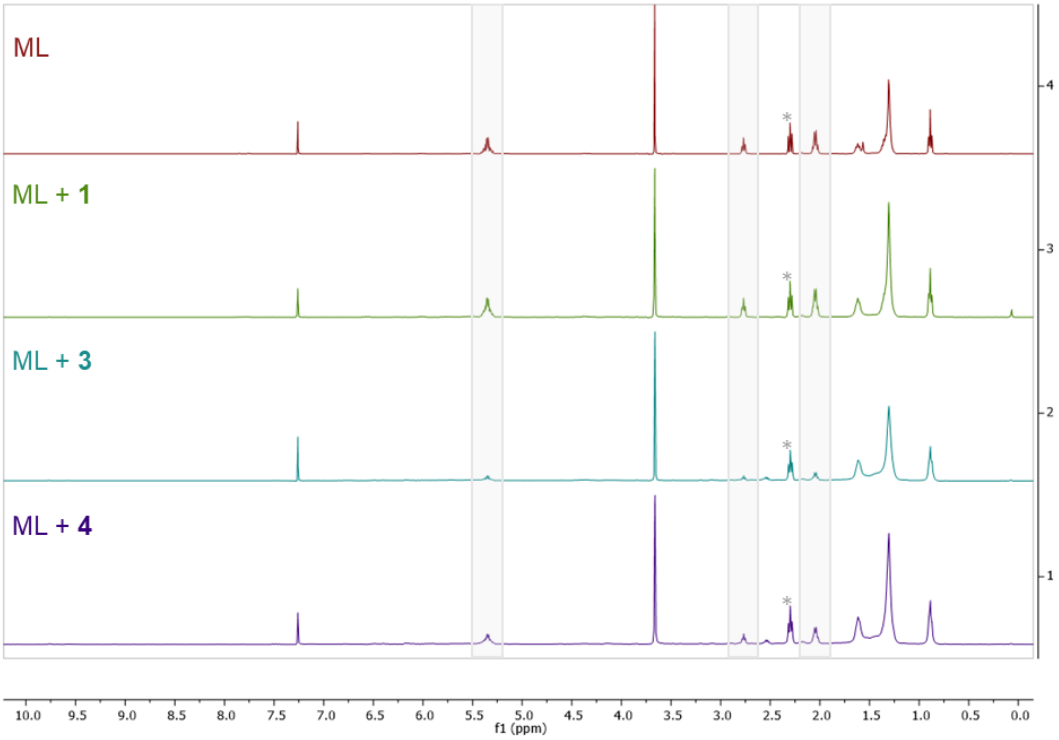

Figure S7. From top to bottom: ^{1}H NMR spectra of methyl linoleate (ML) without catalyst, with [(Cp)Fe(C_6H_6)](PF_6) (**1**), with CoNeo (**3**), and with Mn/MeTACN (**4**). All samples had been exposed to ambient light and air for 6 h prior to analysis. Samples dosed with **3** and **4** show a higher conversion of the non-conjugated *cis*,*cis*-diene motif (highlighted areas). The ester methylene (-C**H**$_2$COOCH$_3$, 2.30 ppm)[6a] has been indicated with an asterisk (*) for reference.

The sample without catalyst shows the presence of conjugated fatty acid hydroperoxides, as indicated by the resonances at 6.64-5.42 ppm belonging to the conjugated diene system[6b] and the resonances at 7.85 and 7.76 ppm belonging to the hydroperoxides.[6a] (Figure S8) Samples with catalyst do not show the resonances corresponding to the hydroperoxides (or in much lower intensity), indicating their consumption. Furthermore, samples with catalysts show formation of aldehydes (9.76 and 9.60 ppm, Figure S8), which are formed *via* β-cleavage of alkoxyl radicals.[6a] Therefore, samples with catalyst show hydroperoxide activation and radical formation typical of fatty acid autoxidation.[6a]

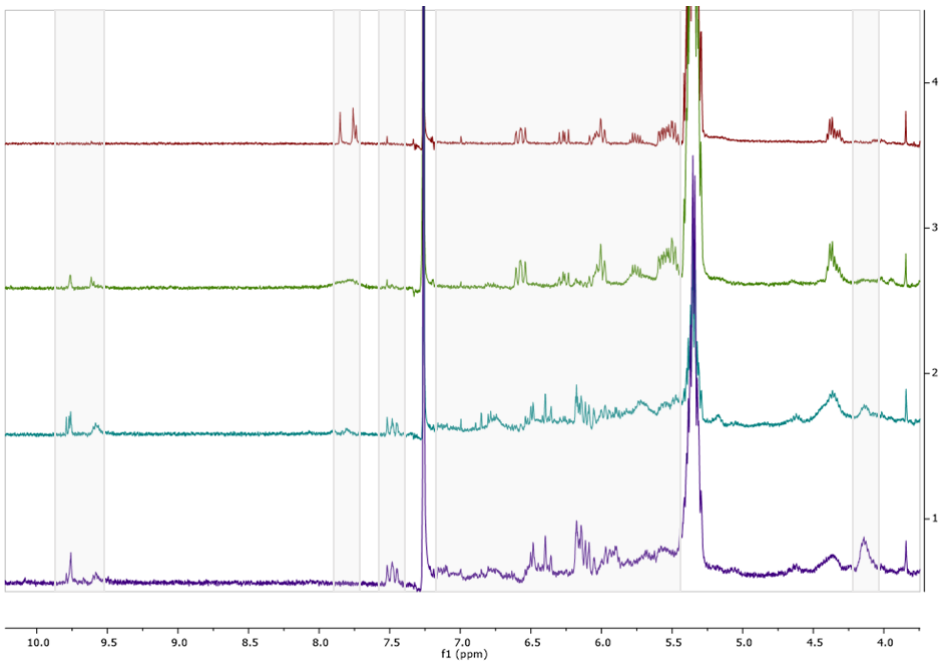

Figure S8. From top to bottom: ^{1}H NMR spectra of methyl linoleate without catalyst, with [(Cp)Fe(C_6H_6)](PF_6) (**1**), with CoNeo (**3**), and with Mn/MeTACN (**4**). All samples had been exposed to ambient light and air for 6 h prior to analysis. The sample with **1** shows reactivity, but the conjugated diene backbone (resonances at 6.64-5.42 ppm) has remained largely intact (central highlighted area); samples with **3** and **4** show the formation of many more species.

Although samples with **3** and **4** show higher conversion than the sample with **1** (Figure S7), they also show the formation of more (side) products. Whereas the sample with **1** still cleanly shows the (partially original, but in higher intensity) conjugated diene backbone, samples with **3** and **4** have developed a much broader palette of resonances in this area during the six hours of the experiment (Figure S8). Furthermore, samples with **3** and **4** show resonances at 7.48 and 4.14 ppm (Figure S8), as well as at 3.20, 3.08 and 2.54 ppm (Figure S9).

Next to reactivity associated with crosslink formation (e.g. radical addition to conjugated dienes), the presence of these additional resonances can indicate the formation of (oxidised) side products. As oxidation has been shown to be linked to degradation in oil paintings (see main text), the nature of these additional species may provide an indication of the specific reactions catalysed by the driers. The competition between molecule oxidation (e.g. epoxidation, hydroxylation) and degradation *vs.* formation of (cross)linked oligomers will be investigated in a follow-up study.

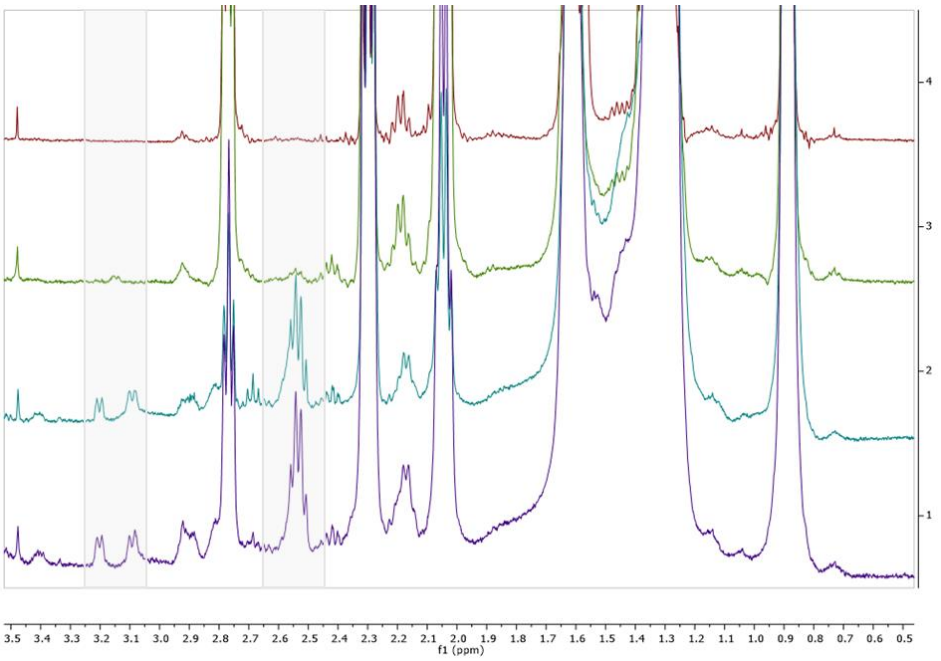

Figure S9. From top to bottom: ^{1}H NMR spectra of methyl linoleate without catalyst, with [(Cp)Fe(C_6H_6)](PF_6) (**1**), with CoNeo (**3**), and with Mn/MeTACN (**4**). All samples had been exposed to ambient light and air for 6 h prior to analysis.

UV/Vis absorption spectroscopy

UV/Vis spectra were recorded on a double beam Shimadzu UV-2600 spectrometer. Paints were prepared on 10 g scale, using 7.90 g Setal-270. For samples containing [(Cp)Fe(C_6H_6)](PF_6) (**1**), the complex was dissolved in acetone before addition to the Setal-270. Additional acetone was subsequently added to a mass of 2.10 g (10.00 g total mass). The following amounts of **1** were used: 0 mg (0.0 wt%), 3.4 mg (0.01 wt%), 6.8 mg (0.02 wt%), 10.2 (0.03 wt%), 13.7 mg (0.04 wt%), 17.1 mg (0.05 wt%), 20.5 mg (0.06 wt%) and 23.9 mg (0.07 wt%). Complex **1** remained soluble in the alkyd mixture up to 0.05 wt%. At 0.06 wt% precipitation took place within a few minutes after mixing, whereas at 0.07 wt% precipitation took place immediately during the mixing process. Only the samples containing 0.00-0.05 wt% loading were used for UV/Vis analysis.

Absorption measurements of the paints were performed in 1.0 cm quartz cuvettes. A baseline spectrum was performed on empty cuvettes, after which the paint without drier (0.0 wt% sample) was measured, followed by the paints with driers. The spectrum of the paint without drier (0.0 wt% sample) was subsequently subtracted from the spectra of paint with driers, to give the spectra as shown in Figure 2 in the main text.

For [(Cp)Fe(Ch)] (**2**) the following amounts were used: 0 mg (0.0 wt%), 4.0 mg (0.02 wt%), 7.9 mg (0.04 wt%), 11.9 mg (0.06 wt%), 15.9 mg (0.08 wt%), 19.8 mg (0.10 wt%), 23.7 mg (0.12 wt%) and 27.8 mg (0.14 wt%). The complex was dosed as a 5.0 wt% solution in heptane, and additional heptane was added to a mass of 2.10 g (10.00 g total mass). Absorption measurements were performed as for paints dosed with **1**.

Absorption spectra of thin films (90 µm) were recorded on glass microscope slides. A baseline spectrum was performed with air, after which a glass slide without paint was measured, followed by the glass slides with paint. The spectrum of the glass slide was subsequently subtracted from the spectra of glass slides with paint. Off-setting all spectra to zero at 600 nm, led to the spectra as shown in Figure S10 below.

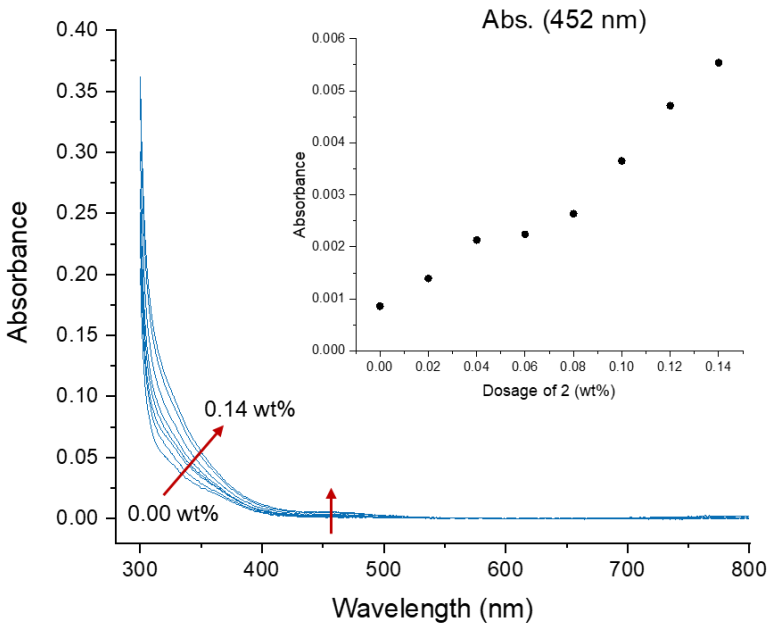

Figure S10. UV/Vis study of 90 µm films of Setal-270 dosed with [(Cp)Fe(Ch)] (0.00-0.14 wt% Fe w.r.t. solid content). The inset is for illustrative purposes only.

Infrared spectroscopy

FTIR spectra were recorded to follow the spectral changes taking place during the curing of Setal-270 with either the commercial driers CoNeo (**3**) and Mn/MeTACN (**4**), or the new [(Cp)Fe(Ch)] / $[(Cp)Fe(C_6H_6)]^+$ system, using on a Spectrum Two FT-IR spectrometer (ATR mode, PerkinElmer) equipped with an UATR accessory. A 90 µm thin film was applied on the ATR crystal using a film applicator and a spectrum was recorded at 15 min intervals during 6 h. Each spectrum was recorded using 16 scans with a spectral resolution of 4 cm^{-1}, in the spectral range of 450-4000 cm^{-1}.

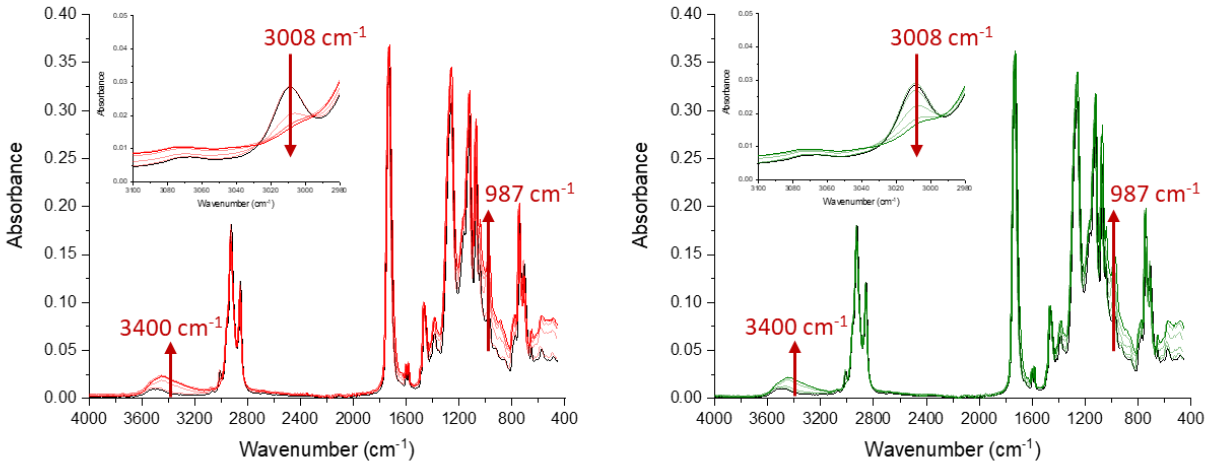

Figure S11. ATR-IR spectra of Setal-270 as it cured using CoNeo (**3**; left) and Mn/MeTACN (**4**; right). Both show the typical[7] changes taking place upon curing: consumption of the *cis*-alkene (3008 cm^{-1}) from the unsaturated fatty acid chains and formation of (conjugated) *trans*-alkene (987 cm^{-1}) as well as an hydroxylated species (3400 cm^{-1}), as for Setal-270 dosed with [(Cp)Fe(Ch)] (**2**) (see Figure 3 in the main text).

To assess whether an intense flash of light is sufficient to activate the complex and thereby start the curing, 90 µm films on glass slides of Setal-270 dosed with **2** at 0.10 wt% were flashed once or multiple times. The glass slides were stored in a dark box and flashed once every

30 minutes using a 500 W flashtube, which gives an intense flash of white light for less than 0.1 s. After each flash the samples were left in the dark for 30 minutes, after which they were analysed by IR spectroscopy. Flashed samples were kept under ambient lighting afterwards and a spectrum was recorded at the end of the experiment. Throughout the whole experiment a set of glass slides was left in the light ('light reference'), of which an IR spectrum was recorded at 30 min intervals.

For these flashbox experiments an FT/IR-4700 FT-IR spectrometer (transmission mode, Jasco) was used, recording spectra in the 2000-4000 cm^{-1} spectral range using 16 scans of 4 cm^{-1} spectral resolution per spectrum. Spectral analysis was performed using the software Spectragryph.[5] The integral values of the absorption band at 3008 cm^{-1} were determined with individual baselining within Spectragryph (integration area: 2992-3030 cm^{-1}). The conversion was determined by comparison to the integral value of the band at 3008 cm^{-1} of a sample prepared without **2**. In these transmission measurements a baseline spectrum was recorded on a glass slide without paint. All measurements were performed in triplo.

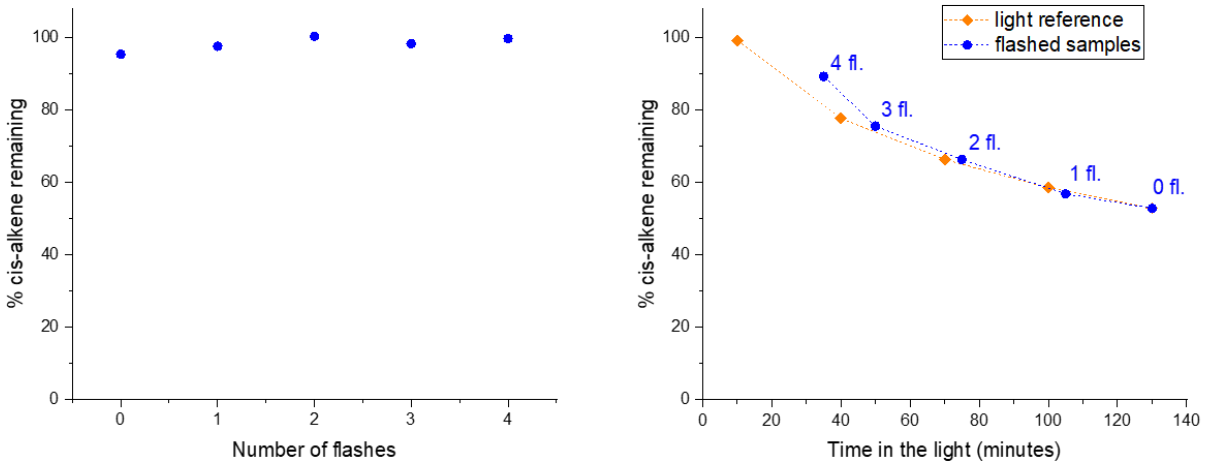

Figure S12. Left: effect of flashes on curing – curing was not observed for single or repeated flashes. Right: curing after flashing – the flashes do not negatively influence the drying, i.e. drying proceeds to the same extent as without intense flashes. After the flashes the samples were left in laboratory light (indoor fluorescent beam lighting + outdoor sunlight through window). Points represent data points, dotted lines have been drawn to guide the eye. Samples which were left in the dark throughout the experiment did not show conversion, as with samples that were only flashed (left).

For the following experiments spectra were recorded using a Nicolet iS50 FT-IR spectrometer (transmission mode, Thermo Scientific), using 16 scans with a spectral resolution of 4 cm^{-1} for each spectrum, the spectra being recorded in the range 2000-4000 cm^{-1}. 90 µm films were applied to glass microscope slides using an applicator cube. In general, 15 min after application the first measurement was performed, and a measurement was performed at 15 minute intervals for 240 minutes (4 h) in total. In these transmission measurements a baseline spectrum was recorded on a glass slide without paint. The conversion was determined by setting the integral value of the 3008 cm^{-1} band (integration area: 2992-3030 cm^{-1}) to 100 for the first spectrum, i.e. conversion = 0 % at t = 15 min. All measurements were performed in duplo.

To test for the effect of storage on curing ability, the curing of several aged samples was followed in time. In these cases, the initial concentrations of *cis*-alkene were determined by ATR-FTIR spectroscopy. Spectra were collected on a Frontier FTIR spectrometer (Perkin-Elmer) equipped with a GladiATR module (Pike Technologies). Spectra were collected with 16 scans and 4 cm^{-1} resolution, in the spectral range 450-4000 cm^{-1}. The band at 3008 cm^{-1} (2992-3030 cm^{-1}) was referenced against the arene bands at ~1600 cm^{-1} (1612-1568 cm^{-1}), taking a sample of Setal-270 without drier as the 100% reference. The initial concentrations decreased to 96 % for 1 day, 93 % for 52 days, 81 % for 289 days and 66 % for 378 days of storage. All samples had been dosed with **2** at 0.10 wt%.

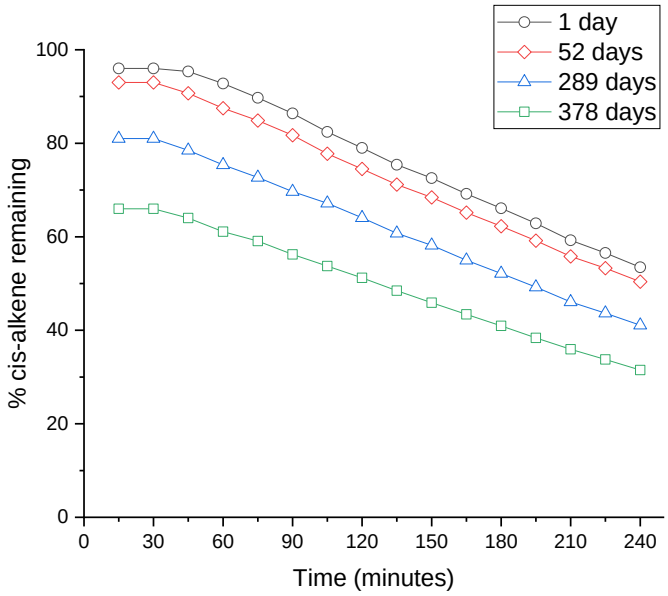

Figure S13. Effect of aging on curing. Linear trendlines were fitted to the data points 60-240 min, the slopes of these indicate a small decrease in conversion rate from 1 day of storage (slope = –0.22) to 52 days of storage (slope = –0.21), and further for 289 days (slope = –0.19) and 378 days (slope = -0.17), all with $R^2 = 0.99$.

All aged samples underwent curing with up to 1 year of storage.

The effect of 2-butanone oxime on curing using **2** was examined (Figure S14).

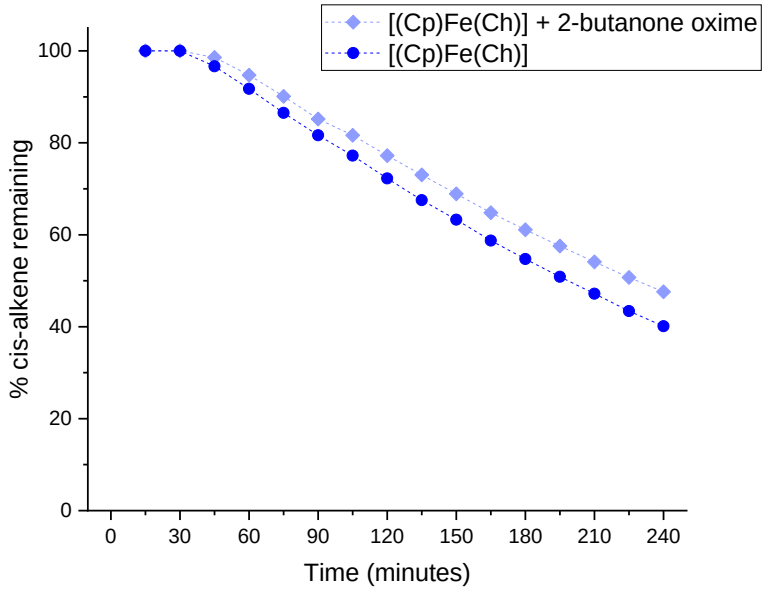

Figure S14. Addition of 2-butanone oxime, an anti-skinning agent often added to alkyd paints containing cobalt and manganese based driers, to Setal-270 dosed with [(Cp)Fe(Ch)] (**2**) at 0.10 wt% has a modest negative effect in the rate of curing (for the period 45-240 min: slope = –0.29 *vs.* slope = –0.26, $R^2 = 0.99$ for paints dosed without and with 2-butanone oxime, respectively). Note that with [(Cp)Fe(Ch)] (**2**) skinning is not observed even upon prolonged storage, even without 2-butanone oxime, i.e. 2-butanone oxime is not required for **2**.

The presence or absence of 2-butanone oxime has only a minor influence on the induction time and reaction rate for alkyd paint curing with [(Cp)Fe(Ch)], and does not affect the overall conversion behaviour.

The effect of concentration of catalyst on curing was examined, the 0.0-0.14 wt% samples of **2** in Setal-270 that were used for the UV/Vis study were also used for an IR study (transmission mode), in which the consumption of *cis*-alkene was followed over time (3008 cm^{-1} band). A reaction order in [Fe] of 0.5 (*rate* = k_{obs}[Fe]$^{0.5}$) was observed (Figure S15).

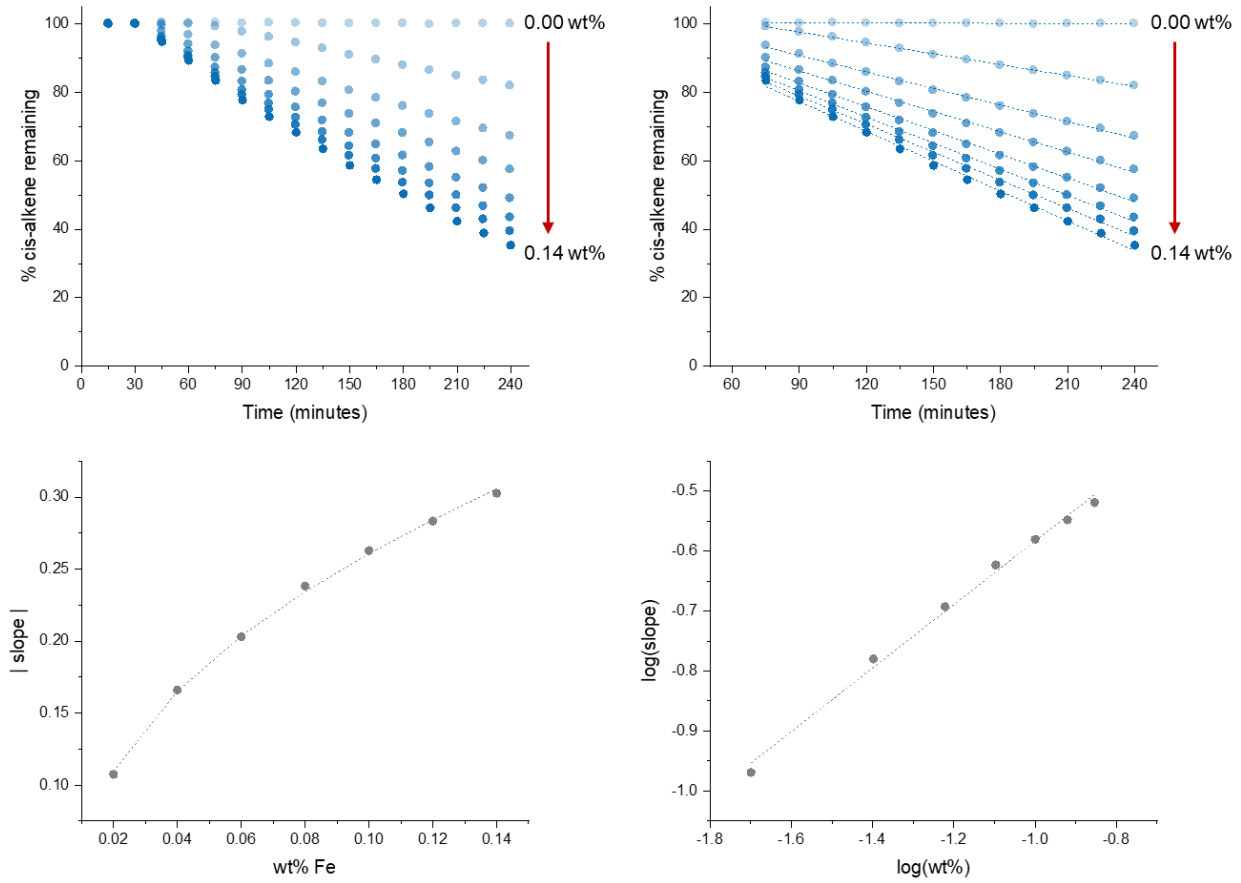

Figure S15. Kinetic study on the effect of concentration of [(Cp)Fe(Ch)] (**2**) in Setal-270 on the consumption of *cis*-alkene (3008 cm^{-1}). After application of 90 µm films on microscope slides, an FTIR spectrum was recorded at 15 min intervals over 4 h (top left). A linear fit of the data from 75-210 min could be made (top right). Plotting these rates (|slope|) *vs.* concentration reveals a logarithmic dependence of the rate of conversion on the dose of **2** (bottom left); a (log, log)-plot suggests a reaction order in [Fe] of 0.5 based on the slope (slope = 0.53, R^2 = 0.99) (bottom right).

Additionally, for further studies a lightbox setup was used, employing a blue LED strip (λ_{em} = 444-498 nm, λ_{max} = 468 nm) with variable light intensity (Figure S16).

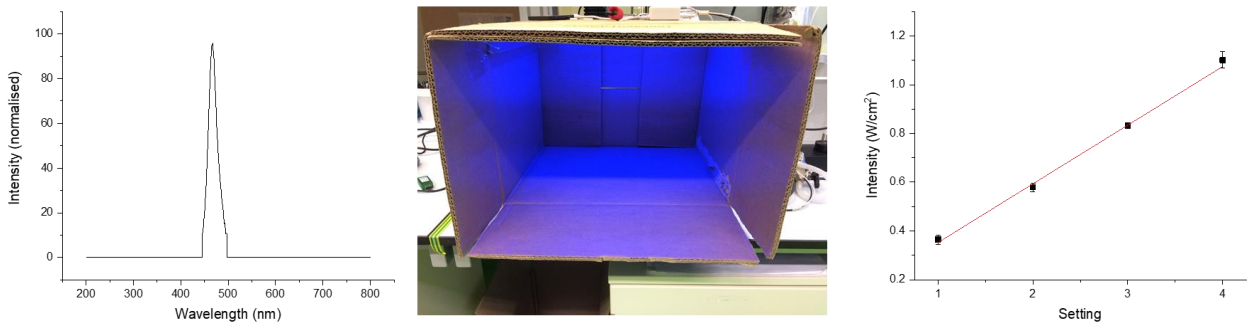

Figure S16. Setup (middle) of the lightbox studies, with (left) the emission spectrum and (right) the intensities of the four settings of the lightbox used (average of 3 measurements). Note: the box was closed from the front during the oxygen / pressure experiments. (The photo in the middle shows the LEDs in action at setting 2.)

The consumption of *cis*-alkene of 90 µm thick paint films (dosed with 0.10 wt% **2**) was also followed by FTIR using these light settings. Firstly, irradiation under setting 1 during 4 hours shows the same linear behaviour (Figure S17, left, closed circles) as that observed under ambient light (Figure 6, main text, and Figure S15). Following the curing for an additional 5 hours reveals an exponential decrease of *cis*-alkene over the 9 hours of the experiment (Figure S17, left, closed circles), reaching 90% conversion over this time.

Additionally, during this experiment samples were taken from the lightbox setup and placed in a shaded area. Samples were taken after 0, 60, 105, 150, 195, 240, 285, 330 and 390 minutes. Next to the light/dark experiment (see main text), where a set of samples was kept alternating in the dark and the light for 30 min intervals, these data also show that curing immediately slows down for samples removed from the light w.r.t. samples that are left in the light (Figure S17, left, open circles). (Continued) curing does take place in the shade, but much slower and with a decreasing rate over time in the dark. An exponential relation was revealed between the percentage of *cis*-alkene remaining and the time spent in the light (Figure S17, right).

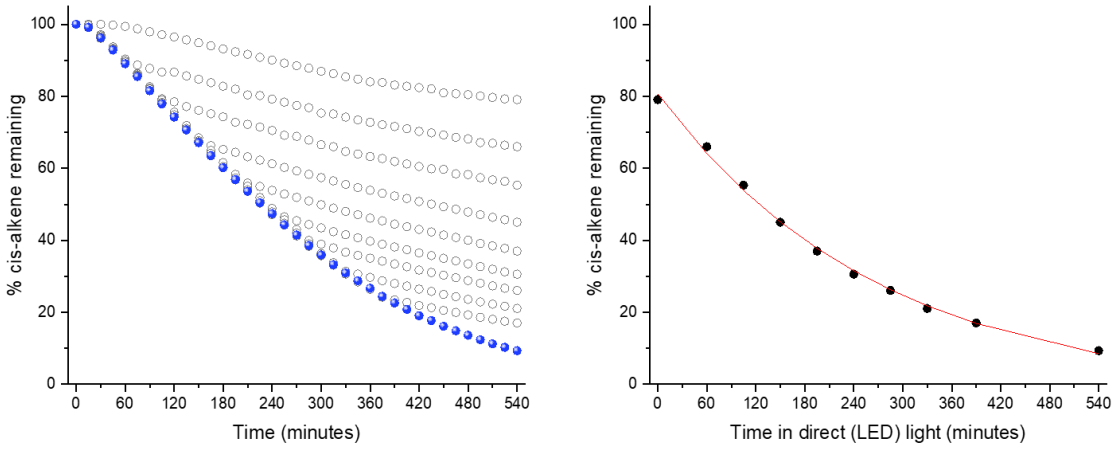

Figure S17. Left: *cis*-alkene conversion for samples under irradiation with lightbox setup (intensity 1; closed circles) and samples moved to a shaded area (open circles). Right: exponential relationship between time in direct light and the percentage of *cis*-alkene remaining (R^2 = 0.99)

Using the four light intensities, the curing of 90 µm thin films dosed with **2** at 0.10 wt% was followed using FTIR spectroscopy.

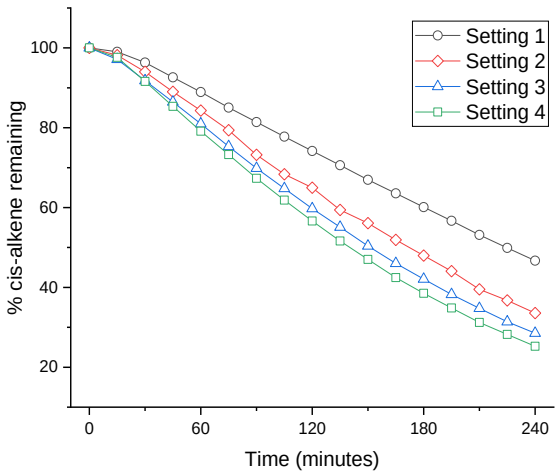

Figure S18. Using the lightbox setup, a correlation was found between the light intensity and the conversion of *cis*-alkene.

The data clearly illustrate that an increase in light intensity leads to an increase in *cis*-alkene conversion.

Furthermore, for all four light intensities kinetic studies suggest a reaction order in [Fe] of 0.5 (Figure S19).

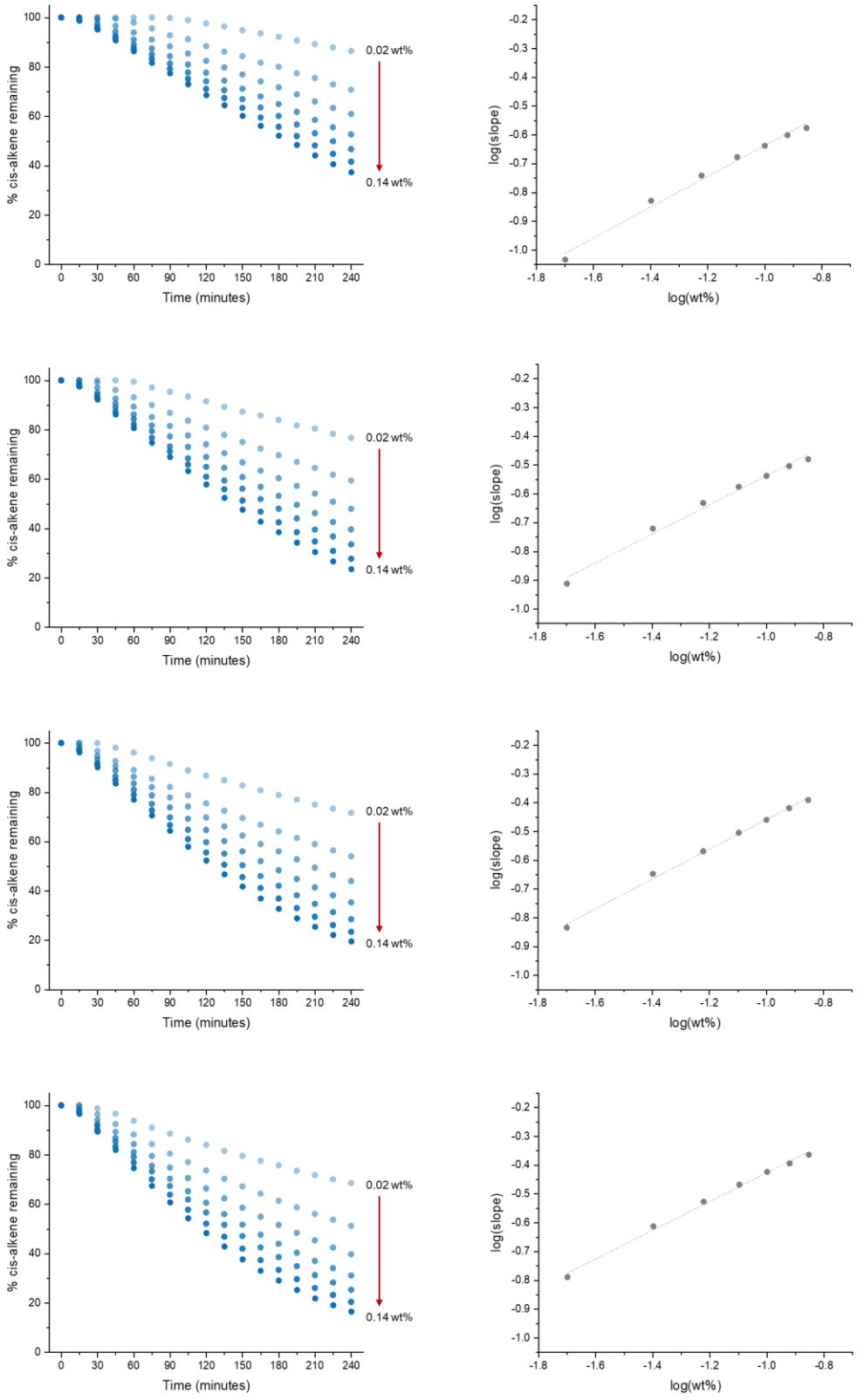

Figure S19. Kinetic study on the effect of concentration of [(Cp)Fe(Ch)] (**2**) in Setal-270 and light intensity (from top to bottom: intensities 1-4 of the lightbox setup) on the consumption of *cis*-alkene (3008 cm^{-1}). After application of 90 µm films on microscope slides, an FTIR spectrum was recorded at 15 min intervals over 4 h (left). A (log, log)-plot between the rate of conversion (obtained from linear fits of the data points) and concentration suggests a reaction order in [Fe] of 0.5 based on the slope of the linear fit (right), as was also revealed from the kinetic study performed under ambient light (Figure S15).

Oxygen consumption

Oxygen consumption by wet paint was followed with both a pressure sensor (Man on the Moon, X102-A08 kit, Universidad Zaragoza) and an optical oxygen meter (FireSting, probe XC7-548-208). (See Figure S20.) Measurements were performed in a closed, tube-shaped flask (1 mL paint, 15 mL air) by levelling the wet paint over the long side of the flask before starting the measurements. The oxygen concentration was measured once every 60 seconds, the pressure was measured once every 10 seconds. The measurements were performed using the lightbox setup (Figure S16).

Figure S20. Oxygen consumption measurements using a pressure sensor (metallic part) and oxygen meter (through septum). Content flask: 16 mL total.

Following the oxygen and pressure change over 6 h revealed an exponential decrease (Figure S21; setting 2 of the lightbox setup).

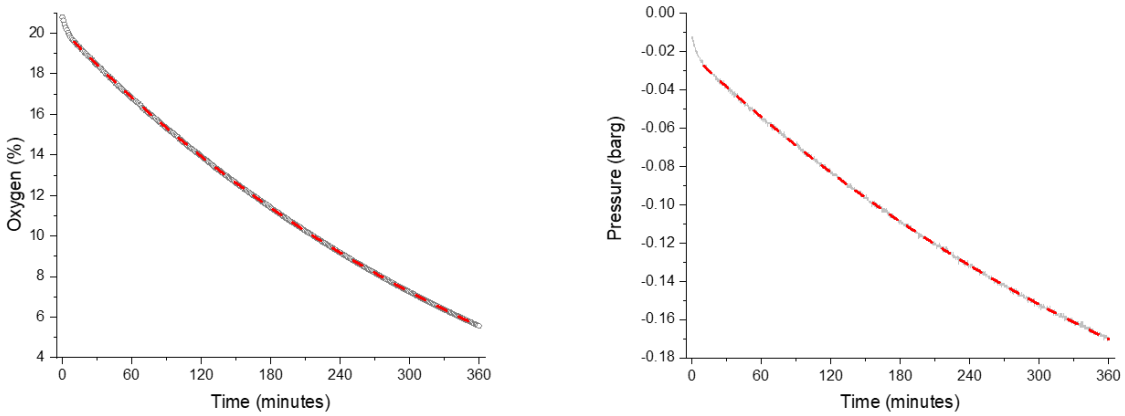

Figure S21. Data points (grey) with exponential fit (red dashed line) of the (left) oxygen concentration and (right) pressure during 6 h under blue LED irradiation (setting 2).

To determine the order in oxygen, the tube was filled with various oxygen concentrations. This was done by adding 1 mL of the wet paint, followed by N_2 gas using a syringe. In this way starting concentrations of 20.8 (0 mL N_2), 16.6 (3 mL N_2), 12.7 (6 mL N_2), 9.5 (10 mL N_2) and 5.9 (16 mL N_2) percent were achieved.

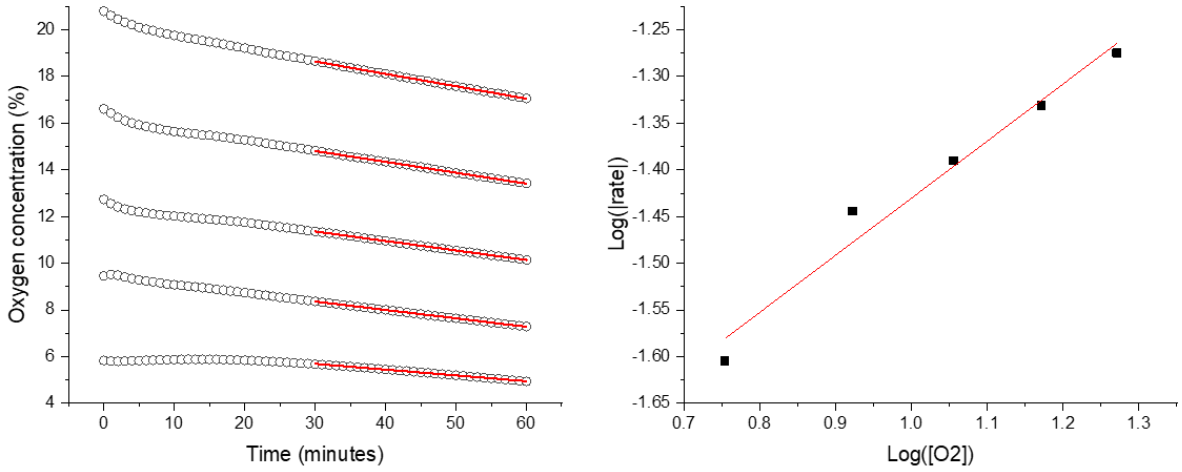

Figure S22. Left: changes in oxygen concentration (open circles), starting from various initial concentrations, with linear trendlines fitted (in red) between 30-60 min (all $R^2 = 0.99$). Right: plotting these rates of oxygen consumption versus the oxygen concentration (at the start of the linear trendline, t = 30 min) in the form of a (log,log)-plot reveals and order in $[O_2]$ of ~0.6 (slope = 0.61, $R^2 = 0.96$).

Plotting log(|rate|) versus log($[O_2]$) reveals an order in $[O_2]$ of ~0.6 (slope = 0.61, $R^2 = 0.96$).

Lastly, the effect of light intensity on the oxygen consumption was investigated. In this experiment the four intensities of the lightbox setup were used. After 105 minutes the light was switched off, and the oxygen concentration followed for an additional 55 minutes.

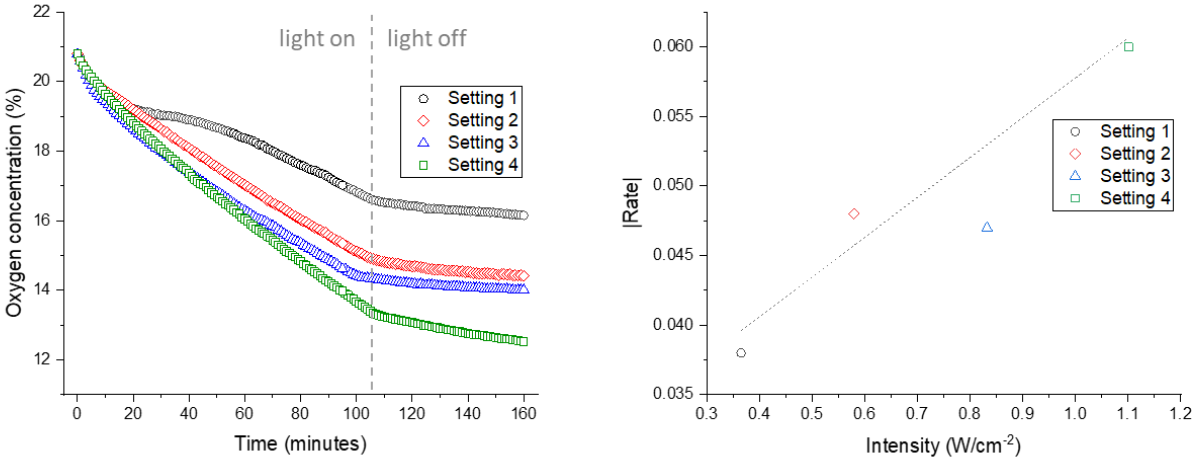

Figure S23. Kinetic study on the effect of light intensity (using the lightbox setup) on oxygen consumption. The LED lights were turned off after 105 min. Using the rates (slopes) as obtained from linear trendline fits on data points 55-95 min (left), a linear trendline fit ($R^2 = 0.96$) for the rates from setting 1, 2 and 4 shows a correlation between light intensity and oxygen consumption (right).

After switching off the light after 105 minutes, the rate in oxygen consumption strongly decreases. That oxygen is still being consumed (although much slower and with a decreasing rate over time in the dark) is in line with the (reduced) consumption of *cis*-alkene in the dark as was observed by FTIR spectroscopy (Figure 4, main text). It seems likely that the radicals formed in the light continue the auto-oxidation process for a while after turning off the light. Furthermore, it seems that the Fe species formed after photoactivation decay into one or more species of low activity, causing some (additional) slow background reactivity in the dark (e.g. peroxide decomposition promoting the auto-oxidation, see also the main text). Here it should be noted though that one or more flashes of light are not enough to start (background) curing (Figure S9), supporting the photo-latency of the system. Furthermore, paint that has been exposed to light and is then stored in the dark over prolonged periods of time does not show skin formation. This suggests that any such low activity Fe species which may be responsible for slow background curing in the dark become fully inactive over a longer period in the dark.

(micro)Raman spectroscopy

Raman spectra were recorded at 785 nm or 632.8 nm. Spectral analysis was carried out using the program Spectragryph.[5]

Raman spectra at 785 nm were recorded with either a RamanFlex instrument (PerkinElmer) equipped with an Inphotonics industrial probe or with a home built Raman microscope (BX51) equipped with a free space laser (75 mW, Ondax, with a 785 nm laser line clean up filter) and dichroic mirror to bring the laser collinear with the optical axis of the microscope. The Raman scattering was collected in backscattering (180°) mode with a Thorlabs fibre launch and round to line bundle of 50 micron fibre optic cable to a Shamrock 163 spectrograph (ANDOR Technology), and dispersed onto a iDUS-420-BUEX2 CCD camera. Spectra were calibrated with polystyrene.[8]

Samples (90 µm thin films) had cured for 5 days before Raman analysis. The spectra were obtained using 10 acquisitions of 5 seconds exposure time for every spectrum. A reference spectrum of Setal-270 was obtained by recording a spectrum after applying a drop of Setal-270 in heptane on a glass plate. A linear baseline correction (1000-1800 cm^{-1} area) was performed for all spectra and the spectra were normalised to the arene band at 1032 cm^{-1} using Spectragryph, resulting in the data shown in Figure 3 in the main text and Figure S24 below.

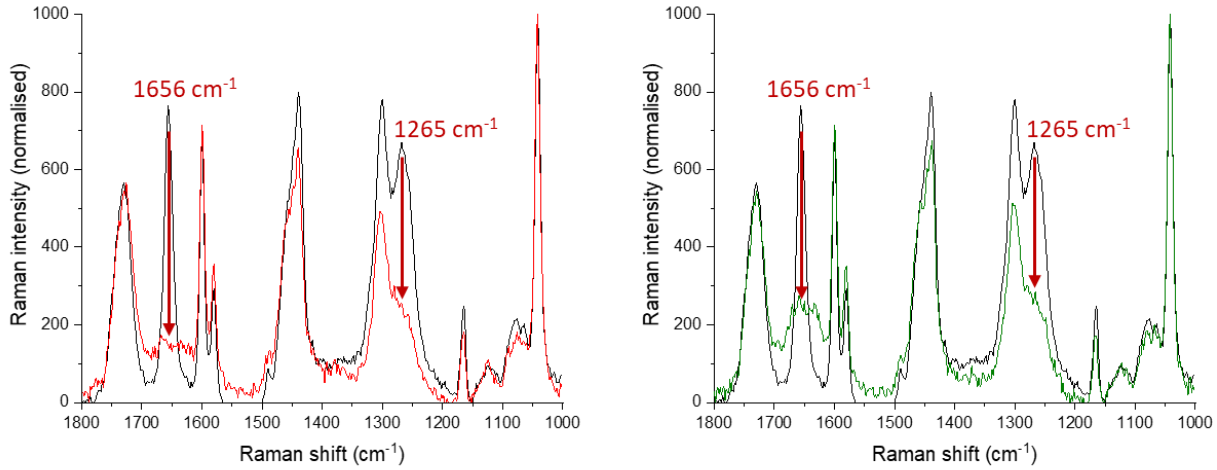

Figure S24. Curing of Setal-270 results in consumption of the alkene CH=CH bands (1265 and 1656 cm^{-1}) of the fatty acid chains, shown here for samples cured with CoNeo (**3**; left) and Mn/MeTACN (**4**; right).

Raman spectra at 632.8 nm (12 mW at source, Cobolt Lasers, typically 3.4 mW at sample) were recorded using an Olympus BX51 uptight microscope and 100x long working distance objective. The excitation light was passed through a polarizing beam splitter, and the power was controlled via a half wave plate and second polarizing beam splitter. The light was directed into the optical path using a dichroic filter, and the Raman scattering was collected through a long pass filter to reject the Rayleigh line. The Raman scattering was focused into a multicore fiber (100 µm, round) to line arrangement and feed into a Shamrock163 spectrograph with an effect slit of ca. 70 µm onto an idus-416 CCD camera (Andor Technology). Data were recorded using Solis (Andor Technology) with spectral calibration performed using the Raman spectrum of polystyrene.[8]

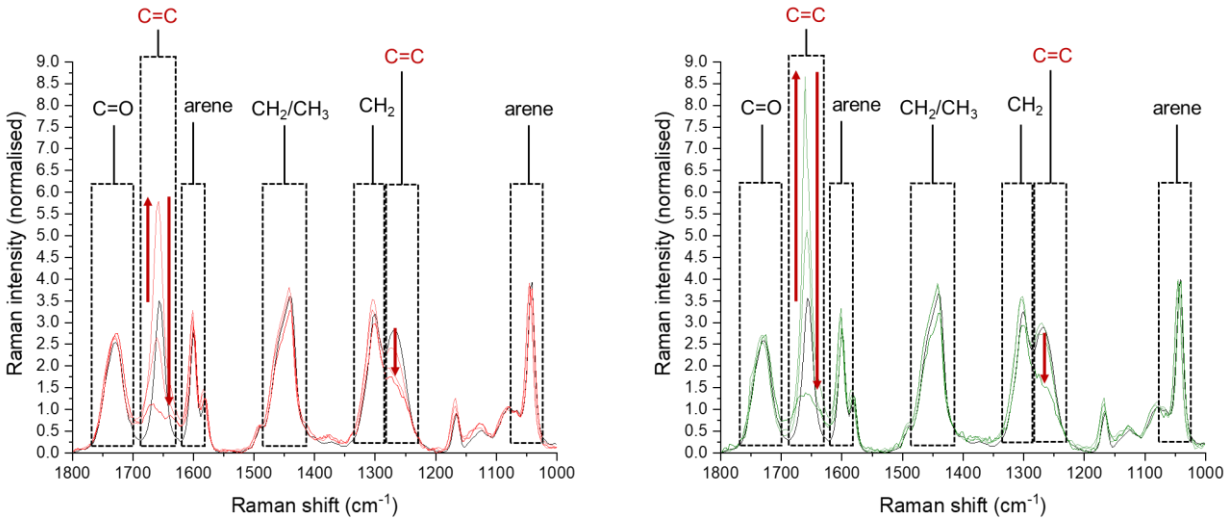

Figure S25. Left: curing of a 90 µm film using CoNeo (**3**) as drier followed by Raman microscopy (λ_{ex} = 633 nm); normalised to the arene vibration 1032 cm^{-1}. Right: the same changes take place when using Mn/MeTACN (**4**).

Depth profiles were measured by applying 150 µm wet films on a quartz plate, which was left in the light for 1 h before the first measurement. For measurements, the plate was placed on the microscope platform. The microscope was focussed on the top of the film, after which the platform was moved up by 10, 30 and 45 µm to get the confocal area at nominal[9] depths of 10, 30 and 45 µm respectively, where spectra were recorded. The spectra at 10 µm nominal depth were recorded using 40 acquisitions of 4 seconds, at 30 µm using 40 acquisitions of 2 seconds, and at 45 µm using 40 acquisitions of 4 seconds for every spectrum. Afterwards the plate was placed back in the light. Repeating this process several times, the curing was followed for five hours. The raw data were analysed by integration of the bands at 1656 cm^{-1} (integration area: 1619-1676 cm^{-1}) and 1032 cm^{-1} (integration area: 1016-1047 cm^{-1}) by using the Integration with Baseline option in Spectragryph. The obtained integrals from the C=C stretching band (1656 cm^{-1}) were normalised to the integral of the arene band (1032 cm^{-1} resonance), yielding the data shown in Figure S26.

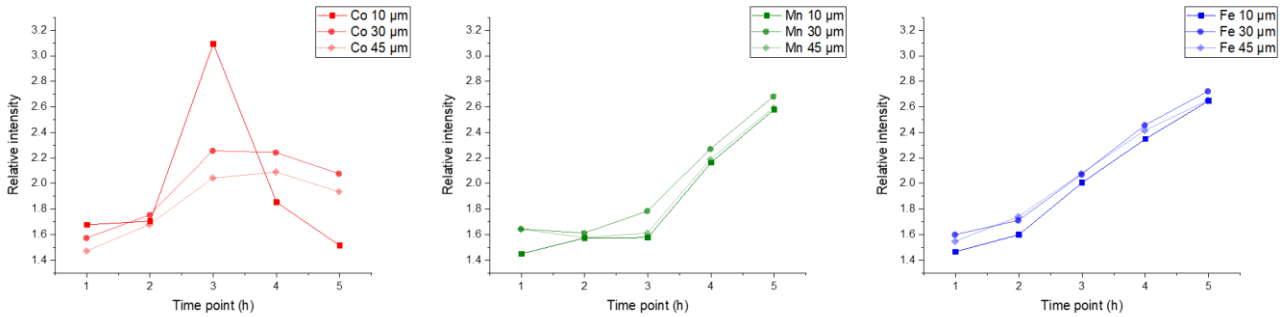

Figure S26. Setal-270 cured with CoNeo (**3**; left), Mn/MeTACN (**4**; middle) and [(Cp)Fe(Ch)] (**2**; right). The driers were dosed at 0.125 wt%, 0.0125 wt% and 0.10 wt%, respectively, as with most of the previous drying studies. CoNeo (**3**) and Mn/MeTACN (**4**) show the front-forming curing and homogeneous curing, respectively, as observed before by Oyman *et al.*;[10] Setal-270 dosed with [(Cp)Fe(Ch)] (**2**) shows homogenous curing just as with Mn/MeTACN (**4**).

Paint dosed with CoNeo (**3**; left) shows front-forming drying: close to the top of the film (10 µm nominal depth) a faster and more intense conversion takes place than deeper in the film (30 and 45 µm nominal depth). For Mn/MeTACN (**4**; middle) homogeneous drying was observed: there is no depth-dependency, i.e. conversion of the starting material takes place equally fast close to the top (10 µm nominal depth) as well as deeper in the film (30 and 45 µm nominal depth) as indicated by the spectral development of the 1656 cm^{-1} band. For paint dosed with [(Cp)Fe(Ch)] (**2**; right) the spectral changes also take place evenly throughout the film, indicating homogeneous drying behaviour for the [(Cp)Fe(Ch)] / [(Cp)Fe(C_6H_6)]$^+$ system.

EPR studies

X-band EPR spectra were recorded on a Bruker EMX-Plus CW X-band EPR spectrometer equipped with an ER 4112HV-CF100 He cryostat. The spectra were analysed and simulated by iteration of the anisotropic g-values, zero-field splitting parameters, (super)hyperfine coupling constants and line widths using the EasySpin module by Stefan Stoll & Arthur Schweiger,[11a] via the cwEPR 3.2 GUI.[11b]

To obtain more information about the fate of Fe-catalyst during the paint curing process, we recorded EPR spectra of a freshly dried paint layer. The paint layer was removed from a glass plate after 24h curing, and an EPR tube was filled with the thus obtained paint flakes. EPR spectra of the closed tube were recorded at 20 K. The resulting spectrum is shown in Figure S27.

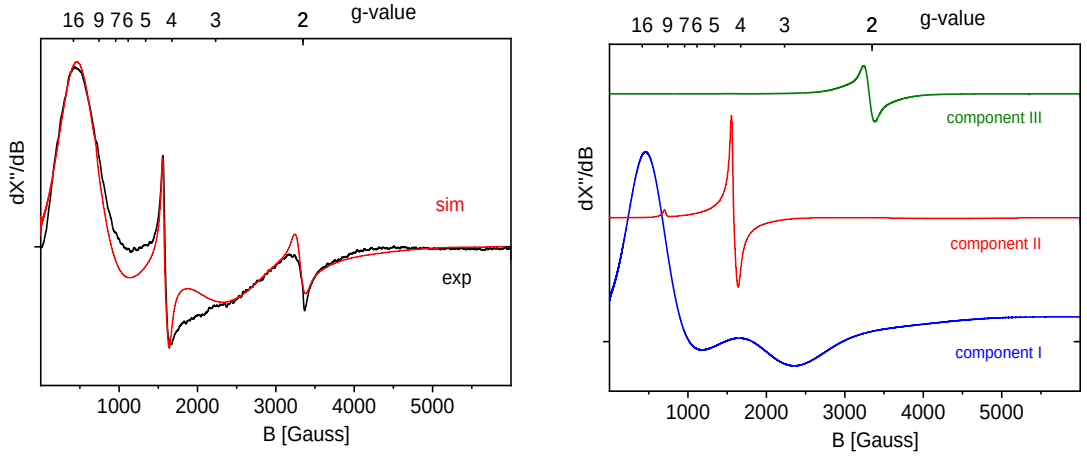

Figure S27. Left: Experimental and simulated EPR spectrum of paint flakes obtained after 24 h curing with [(Cp)Fe(Ch)] **2**. Experimental conditions: T = 20 K; Freq. = 9.369569 GHz ; Mod. Ampl. = 4 G, microwave power = 2 mW. Simulation parameters are shown in Table S2. Right: Individual spectra of the three components (**I**, **II** and **III**) contributing to the simulated spectrum.

The spectrum is composed of three components (**I**, **II** and **III**). The main broad signal (component **I**) with effective g-values of ~10 and ~3 can be simulated with an S = 2 spin Hamiltonian with a large zero field splitting parameter (D > hν) and a small E/D rhombicity parameter, which is characteristic for high spin Fe(II) species.[12] A similar S = 2 signal, most likely stemming from a high spin $[(Cp)Fe(solv)]^+$ species generated by photo-triggered benzene loss from $[(Cp)Fe(benzene)]^+$, was detected upon exposing a frozen anaerobic THF solution of the diamagnetic complex $[(Cp)Fe(benzene)](PF_6)$ to UVA-visible light (range 320-500 nm) in the EPR cavity using a powerful fiber optics lamp (see Figure S28 and Table S2).

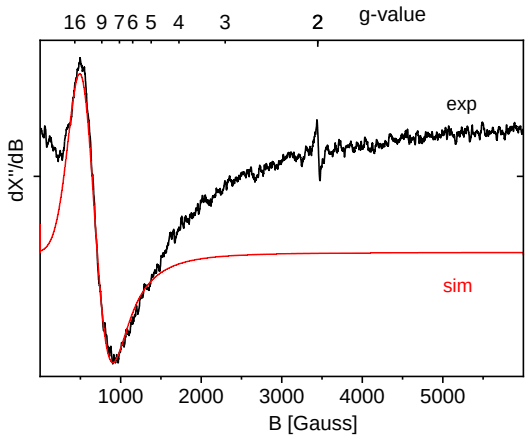

Figure S28. Experimental and simulated EPR spectrum of $[(Cp)Fe(benzene)](PF_6)$ exposed to a visible light range 320-500 nm in the EPR cavity. $[(n\text{-}Bu)_4N]PF_6$ was added to obtain a better glass. Experimental conditions: T = 20 K; Freq. = 9.649761 GHz ; Mod. Ampl. = 4 G, microwave power = 0.632 mW. Simulation parameters are shown in Table S2.

The combined results suggest that [(Cp)Fe(Ch)] / $[(Cp)Fe(C_6H_6)]^+$ converts to a high spin (S = 2) Fe(II) species in the alkyd matrix upon exposure to ambient light during paint curing, plausibly a $[(Cp)Fe]^+$ cation bound to the ester and/or carboxylate moieties of the alkyd medium. However, di- or multinuclear clusters with an (effective) S = 2 spin ground state cannot be fully excluded.[13]

Table S2. EPR parameters used in the simulations.

	spin	g-values (g_x=g_y=g_z)	[D, E] (E/D) (MHz)	D-strain (MHz)	H-strain (MHz)
Component I	S = 2	2.050	[350e³, 1510] (0.0043)	-	[280, 100, 750]
Component II	S = 5/2	1.960	[200e³, 64e³] (0.32)	-	[6500, 300, 100]
Component III	S = 5/2	2.025	[400, 0] (0)	[600, 400]	[200, 600, 200]
$[(Cp)Fe(solv)]^+$	S = 2		[300e³, 1515] (0.0051)	-	[200, 700, 700]

The other two components (**II** and **III**) detected in the EPR spectrum of the freshly dried paint sample (Figure S27) are characteristic for small amounts of high spin Fe(III) S = 5/2 spin centers. Similar signals have been observed in EPR spectra of dendrimer supported Fe_2O_3 nanoparticles.[14] The signal with an effective g-value of ~4.3 (component **II**) has a large zero field splitting D > hν and a large rhombicity parameter E/D ~1/3 (Table S2). Such signals can be assigned to high spin Fe(III) ions in a tetrahedral environment.[14] The signal with an effective g-value close to ~2 (component **III**) has a weak axial zero field splitting parameter D << hν (E/D = 0), observed for Fe(III) ions in an octahedral environment with a weakly distorted crystal field in Fe_2O_3.[14]

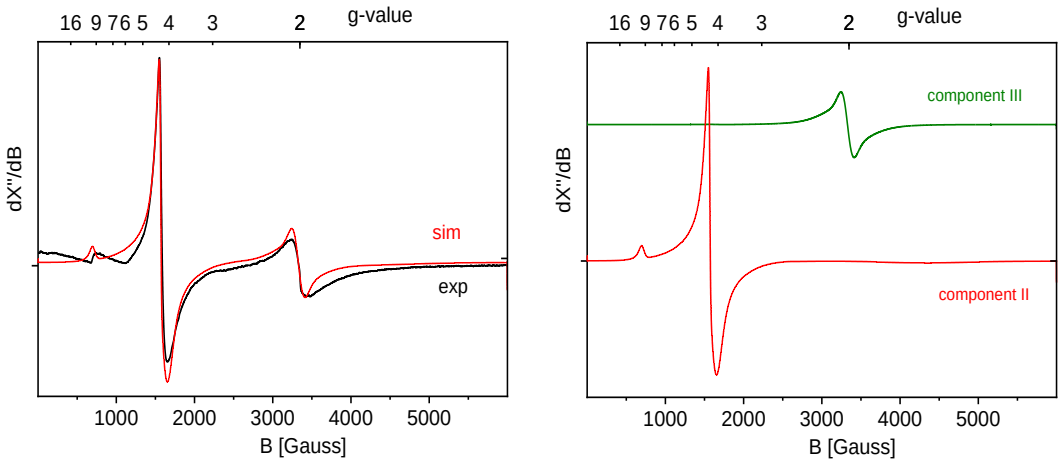

Figure S29. Left: Experimental and simulated EPR spectrum of paint flakes obtained after several weeks curing with the [(Cp)Fe(Ch)] / $[(Cp)Fe(C_6H_6)]^+$ system. Experimental conditions: T = 20 K; Freq. = 9.372460 GHz ; Mod. Ampl. = 4 G, microwave power = 2 mW. Simulation parameters are shown in Table S2. Right: Individual spectra of the two components (**II** and **III**) contributing to the simulated spectrum.

Upon prolonged curing, the relative intensity of the EPR signals of components **I**, **II** and **III** in the cured paint changes. In paint samples cured for several weeks the S = 2 Fe(II) signal component **I** is no longer detectable, while the S = 5/2 Fe(III) signals (components **II** and **III**) have increased in intensity (Figure S29). Simulation reveals identical spin Hamiltonian parameters as obtained for components **II** and **III** in the freshly cured paint sample (Table S2). Based on the similarities between the measured EPR signals in the cured paint samples and those detected in EPR spectra of dendrimer supported Fe_2O_3 nanoparticles[14] it is tempting to conclude that upon prolonged curing the high spin Fe(II) species detected in the freshly cured paint (1 day) convert slowly (several days to weeks) to Fe_2O_3. However, formation of other (e.g. mononuclear) high spin Fe(III) species cannot be fully excluded. In contrast to the reported dendrimer supported γ-Fe_2O_3 oxide nanoparticles, the Fe(III) signals detected in the cured paint layers do not show superparamagnetic behaviour; except for expected broadening, the relative intensities and peak positions do not change when the samples are recorded at RT.

To probe the (radical) mechanism, spin-trapping experiments were performed. For these experiments a solution of 3.00 g Setal-270 in 7.00 g benzene (without or with Fe, 10.0 mg **2**) was degassed by four freeze-pump-thaw cycles before it was introduced into a N_2-filled glovebox. Two solutions were prepared: 40 mg phenyl-*N*-t-butylnitrone (PBN) in 2.4 mL Setal-270 solution in benzene (without Fe), and 32 mg 5,5-dimethyl-1-pyrrolidine-N-oxide (DMPO) in 2.4 mL Setal-270 solution in benzene (without Fe). Of each solution, 1.1 mL was transferred to

a vial (2x). To each vial was added 1.1 mL Setal-270 in benzene solution (without or with Fe). In this way four vials were prepared: PBN without Fe, PBN with Fe, DMPO without Fe, and DMPO with Fe. Of each solution was transferred 0.6 mL to an EPR tube; parafilm was used to close-off the cap/tube. The remainder of the solutions was taken outside the glovebox, mixed by pipette in air, and 0.6 mL of these air-mixed solutions was transferred to an EPR tube. In total eight EPR samples were prepared. Samples were measured at room temperature, using a modulation amplitude of 2 G and a microwave power of 0.6325 mW.

The control samples without **2** already showed a very weak EPR signal, both for samples air-mixed or those under N_2-atmosphere, which increased slightly over ~2 h under ambient lighting. Samples dosed with **2** showed the same spectral features, but with a markedly increased intensity (Figure S30).

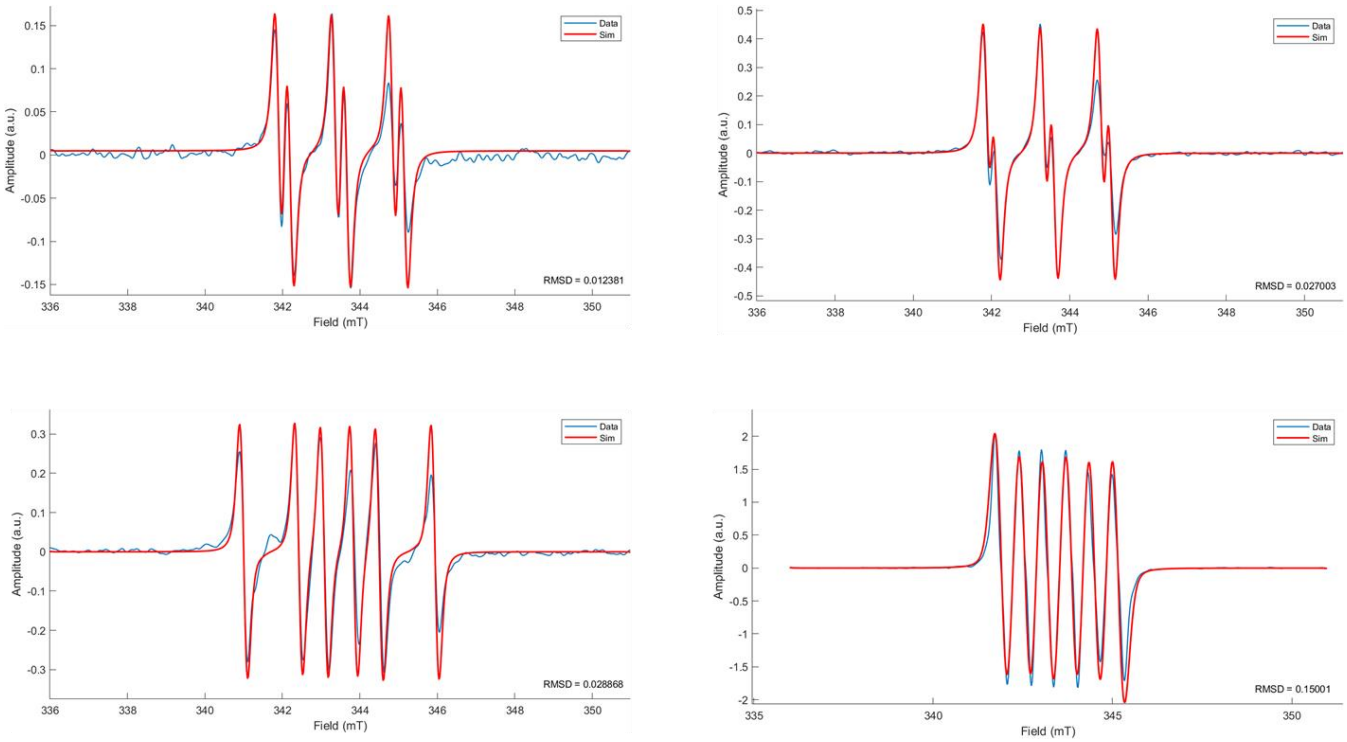

Figure S30. Experimental and simulated EPR spectrum of solutions of Setal-270 with **2** and spin-traps PBN (top) or DMPO (bottom). Experiments were performed under N_2-atmosphere (left) or air (right). Simulation parameters are shown in Table S3.

In the case of PBN a distinction could not be made between the radicals trapped under N_2 (a_N = 14.76 G, a_H = 2.99 G) or air atmosphere (a_N = 14.68 G, aH = 2.55 G). (Simulation parameters are shown in Table S3.) Fitting of the DMPO spectra revealed that C-centered radicals (aN = 14.25 G, aH = 20.88 G) are trapped for the sample under N_2, while O-centered radicals (aN = 12.99 G, aH = 6.66 G) are trapped for the sample under aerobic conditions. These trapped species originate from a conjugated fatty acid diene radical and a conjugated diene alkoxyl radical, respectively.[15]

Table S3. EPR parameters used in the simulations for the solutions Fe + spin-trap

	Freq. (GHz)	g-values (g_x=g_y=g_z)	a_N (MHz)	A_H (Mhz)	a_N (G)	a_H (G)
PBN, under N_2	9.643932	2.0058	41.43	8.39	14.76	2.99
PBN, under air	9.642503	2.0058	41.21	7.16	14.68	2.55
DMPO, under N_2	9.642057	2.0057	39.99	58.62	14.25	20.88
DMPO, under air	9.644115	2.0058	36.47	18.70	12.99	6.66

References in the Electronic Supporting Information

(1) Almas, A. I.; Singh, A. J.; Spencer, J. L. Synthesis and Reactions of Ferrocene, Magritek Lab Manual (https://www.magritek.com/wpcontent/uploads/2015/03/Lab-Manual-Synthesis-and-Reactions-of-Ferrocene-web.pdf)

(2) Sutherland, R. G.; Zhang, C. H.; Chowdhury, R. L.; Píorko, A.; Lee, C. C. Product Distributions in the Addition of the Hydride Ion to Cyclopentadienyliron Complexes of Substituted Benzenes. *J. Organomet. Chem.*, **1987**, *3*, 367-381.

(3) Wieghardt, K.; Bossek, U.; Nuber, B.; Weiss, J.; Bonvoisin, J.; Corbella, M.; Vitols, S. E.; Girerd, J.J. Manganese(II), -(III), and –(IV) of Biological Relevance. The Crystal Structure of $[L'Mn^{IV}(\mu\text{-}O)_3Mn^{IV}L'](PF_6)_2 \bullet H_2O$ Containing an Unprecedented Short Mn•••Mn Distance of 2.296 Å. *J. Am. Chem. Soc.* **1988**, *110*, 7398-7411.

(4) Simpson, N.; Maaijen, K.; Roelofsen, Y.; Hage, R. The Evolution of Catalysis for Alkyd Coatings: Responding to Impending Cobalt Reclassification with Very Active Iron and Manganese Catalysts, Using Polydentate Nitrogen Donor Ligands. *Catalysts* **2019**, *9*, 825.

(5) Spectragryph; Spectroscopy Ninja, 2016; http://spectragryph.com

(6) (a) Miccichè, F; van Haveren, J.; Oostveen, E.; Ming, W.; van der Linde, R. Oxidation and Oligomerization of Ethyl Linoleate Under the Influence of the Combination of Ascorbic Acid 6-palmitate / Iron-2-ethylhexanoate, *Appl. Catal. A: Gen.*, **2006**, *297*, 174-181. (b) Lie Ken Jie, M. S. F. Analysis of Conjugated Linoleic Acid Esters by Nuclear Magnetic Resonance Spectroscopy. *Eur. J. Lipid Sci. Technol.*, **2001**, *103*, 628-632.

(7) van de Voort, F. R.; Ismail, A. A.; Sedman, J.; Emo, G. Monitoring the Oxidation of Edible Oils by Fourier Transform Infrared Spectroscopy. *J. Am. Oil. Chem. Soc.*, **1994**, *71*, 243-253.

(8) McCreery, R. L. in *Raman Spectroscopy for Chemical Analysis*, John Wiley & Sons, Inc., New York, **2000**, Ch. 10.

(9) (a) Everall, N. Depth Profiling with Confocal Raman Microscopy, Part I. *Spectroscopy*, **2004**, *10*, 22-28. (b) Everall, N. Depth Profiling with Confocal Raman Microscopy, Part II. *Spectroscopy*, **2004**, *11*, 16-26.

(10) Oyman, Z. O.; Ming, W.; van der Linde, R.; ter Borg, J.; Schut, A.; Bieleman, J. H. Oxidative Drying of Alkyd Paints Catalysed by a Dinuclear Manganese Complex (MnMeTACN). *Surface Coatings International Part B: Coatings Transactions* **2005**, *88*, 269-275.

(11) (a) Stoll, S.; Schweiger, A.; EasySpin, a comprehensive software package for spectral simulation and analysis in EPR. *J. Magn. Reson.* **2006**, *178(1),* 42-55. (b) Thomas Casey (2021). cwEPR, MATLAB Central File Exchange (https://www.mathworks.com/matlabcentral/fileexchange/73292-cwepr).

(12) (a) Hendrich, M. P.; Debrunner, P. G. Integer-Spin Electron Paramagnetic Resonance or Iron Proteins. *Biophys. J.* **1989**, *56*, 489-506. (b) Andres, H.; Bominaar, E. L.; Smith, J. M.; Eckert, N. A.; Holland, P. L.; Münck, E. Planar Three-Coordinate High-Spin Fe^{II} Complexes with Large Orbital Angular Momentum: Mössbauer, Electron Paramagnetic Resonance, and Electronic Structure Studies. *J. Am. Chem. Soc.* **2002**, *124*, *12*, 3012–3025.

(13) Hendrich, M. P.; Münck, E.; Fox, B. G.; Lipscomb, J. D. Integer-Spin EPR Studies of the Fully Reduced Methane Monooxygenase Hydroxylase Component. *J. Am. Chem. Soc.* **1990**, *112*, 5861–5865.

(14) Gruzdev, M. S.; Chervonova, U. V.; Vorobeva, V. E.; Ksenofontova, A. A.; Kolkera, A. M. Liquid crystalline poly(propylene imine) dendrimer-based iron oxide nanoparticles. *RSC Adv.* **2019**, *9*, 22499–22512.

(15) Pryor, W. A.; Prier, D. G.; Church, D. F. Radical Production from the Interaction of Ozone and PUFA as Demonstrated by Electron Spin Resonance Spin-Trapping Techniques. *Environmental Research*, **1981**, *24*, 42-52.

[1] Almas, A. I.; Singh, A. J.; Spencer, J. L. Synthesis and Reactions of Ferrocene, Magritek Lab Manual (https://www.magritek.com/wp-content/uploads/2015/03/Lab-Manual-Synthesis-and-Reactions-of-Ferrocene-web.pdf)
[2] Sutherland, R. G.; Zhang, C. H.; Chowdhury, R. L.; Píorko, A.; Lee, C. C. Product Distributions in the Addition of the Hydride Ion to Cyclopentadienyliron Complexes of Substituted Benzenes. *J. Organomet. Chem.*, **1987**, *3*, 367-381.
[3] Wieghardt, K.; Bossek, U.; Nuber, B.; Weiss, J.; Bonvoisin, J.; Corbella, M.; Vitols, S. E.; Girerd, J.J. Manganese(II), -(III), and –(IV) of Biological Relevance. The Crystal Structure of $[L'Mn^{IV}(\mu\text{-}O)_3Mn^{IV}L'](PF_6)_2 \bullet H_2O$ Containing an Unprecedented Short Mn•••Mn Distance of 2.296 Å. *J. Am. Chem. Soc.* **1988**, *110*, 7398-7411.
[4] Simpson, N.; Maaijen, K.; Roelofsen, Y.; Hage, R. The Evolution of Catalysis for Alkyd Coatings: Responding to Impending Cobalt Reclassification with Very Active Iron and Manganese Catalysts, Using Polydentate Nitrogen Donor Ligands. *Catalysts* **2019**, *9*, 825.
[5] Spectragryph; Spectroscopy Ninja, 2016; http://spectragryph.com
[6] (a) Miccichè, F; van Haveren, J.; Oostveen, E.; Ming, W.; van der Linde, R. Oxidation and Oligomerization of Ethyl Linoleate Under the Influence of the Combination of Ascorbic Acid 6-palmitate / Iron-2-ethylhexanoate, *Appl. Catal. A: Gen.*, **2006**, *297*, 174-181. (b) Lie Ken Jie, M. S. F. Analysis of Conjugated Linoleic Acid Esters by Nuclear Magnetic Resonance Spectroscopy. *Eur. J. Lipid Sci. Technol.*, **2001**, *103*, 628-632.
[7] van de Voort, F. R.; Ismail, A. A.; Sedman, J.; Emo, G. Monitoring the Oxidation of Edible Oils by Fourier Transform Infrared Spectroscopy. *J. Am. Oil. Chem. Soc.*, **1994**, *71*, 243-253.
[8] McCreery, R. L. in *Raman Spectroscopy for Chemical Analysis*, John Wiley & Sons, Inc., New York, **2000**, Ch. 10.
[9] (a) Everall, N. Depth Profiling with Confocal Raman Microscopy, Part I. *Spectroscopy*, **2004**, *10*, 22-28. (b) Everall, N. Depth Profiling with Confocal Raman Microscopy, Part II. *Spectroscopy*, **2004**, *11*, 16-26.
[10] Oyman, Z. O.; Ming, W.; van der Linde, R.; ter Borg, J.; Schut, A.; Bieleman, J. H. Oxidative Drying of Alkyd Paints Catalysed by a Dinuclear Manganese Complex (MnMeTACN). *Surface Coatings International Part B: Coatings Transactions* **2005**, *88*, 269-275.
[11] (a) Stoll, S.; Schweiger, A.; EasySpin, a comprehensive software package for spectral simulation and analysis in EPR. *J. Magn. Reson.* **2006**, *178(1),* 42-55. (b) Thomas Casey (2021). cwEPR, MATLAB Central File Exchange (https://www.mathworks.com/matlabcentral/fileexchange/73292-cwepr).
[12] (a) Hendrich, M. P.; Debrunner, P. G. Integer-Spin Electron Paramagnetic Resonance or Iron Proteins. *Biophys. J.* **1989**, *56*, 489-506. (b) Andres, H.; Bominaar, E. L.; Smith, J. M.; Eckert, N. A.; Holland, P. L.; Münck, E. Planar Three-Coordinate High-Spin Fe^{II} Complexes with Large Orbital Angular Momentum: Mössbauer, Electron Paramagnetic Resonance, and Electronic Structure Studies. *J. Am. Chem. Soc.* **2002**, *124*, *12*, 3012–3025.
[13] Hendrich, M. P.; Münck, E.; Fox, B. G.; Lipscomb, J. D. Integer-Spin EPR Studies of the Fully Reduced Methane Monooxygenase Hydroxylase Component. *J. Am. Chem. Soc.* **1990**, *112*, 5861–5865.
[14] Gruzdev, M. S.; Chervonova, U. V.; Vorobeva, V. E.; Ksenofontova, A. A.; Kolkera, A. M. Liquid crystalline poly(propylene imine) dendrimer based iron oxide nanoparticles. *RSC Adv.* **2019**, *9*, 22499–22512.
[15] Pryor, W. A.; Prier, D. G.; Church, D. F. Radical Production from the Interaction of Ozone and PUFA as Demonstrated by Electron Spin Resonance Spin-Trapping Techniques. *Environmental Research*, **1981**, *24*, 42-52.